AIMS Materials Science, 13(1): 30–61.
DOI: 10.3934/matersci.2026002
Received: 25 October 2025
Revised: 04 December 2025
Accepted: 12 December 2025
Published: 08 January 2026

https://www.aimspress.com/journal/Materials

Review

Application of DC plasma torches for spheroidization processes of irregularly shaped powders

Volodymyr Korzhyk[1,2], Dmytro Strohonov[2,*], Oleksii Tereshchenko[2], Sviatoslav Peleshenko[2], Oleg Ganushchak[2], Oleksii Demianov[2], Zhenlong Li[1,*] and Yu Chen[2]

[1] China-Ukraine Institute of Welding, Guangdong Academy of Sciences, Guangdong Provincial Key Laboratory of Material Joining and Advanced Manufacturing: 363, Changxing Road, Tianhe, Guangzhou, 510650, China

[2] E.O. Paton Electric Welding Institute, National Academy of Sciences of Ukraine, 11 Kazymyr Malevych St., 03150 Kyiv, Ukraine

* **Correspondence:** Email: strogonovd94@gmail.com; lizhl@gwi.gd.cn.

Abstract: The article presents a review of modern designs of direct current arc plasma torches and the technological configurations used for plasma spheroidization of irregularly shaped powders. The study examines plasma torch designs employing both "hot" thermionic tungsten electrodes and "cold" autoemissive copper electrodes, demonstrating their ability to operate with various types of plasma-forming gas mixtures. The influence of the plasma-forming gas's composition on the electrode erosion intensity is analyzed, and approaches to improving the electrode's lifetime and overall torch reliability are outlined. The processes of particle heating, melting, and spheroidization are examined, along with the key parameters determining spheroidization efficiency: Plasma enthalpy and velocity, particle size, residence time in the high-temperature zone, and the powder feeding scheme. It is shown that radial feeding provides 70%–82% spherical particles, and up to 86%–97% under high-power operating conditions. Axial feeding achieves more than 95% spheroidized particles. Promising technological solutions aimed at increasing the productivity of the spheroidization of ceramic and metallic materials are also discussed.

Keywords: plasma spheroidization; direct current arc plasma torches; radial feed; axial feed; powder; sphericity; degree of spheroidization; energy efficiency

1. Introduction

In modern materials science, there is a growing interest in high-tech methods for modifying the shape, structure, and chemical composition of powder materials, particularly using plasma spheroidization methods [1,2]. Spheroidized powders have a number of advantages over irregular particles: improved fluidity, bulk density, better packing capacity, and, as a result, better mechanical and operational properties of the final products [3,4]. Currently, spheroidization of irregularly shaped powders is a particularly relevant task for additive manufacturing technologies using metallic and ceramic materials, where there is an urgent need to improve the technological properties of powders obtained by mechanical, chemical, electrochemical methods, gas atomization of melts, etc. [5–8]. Thus, in other works [2,5–7,9–11], it is noted that plasma spheroidization is an effective way to improve the sphericity, fluidity, bulk density, and other characteristics of powders from a wide range of metals and alloys such as 100Cr6, Fe23Cr11Mn1N, SS 304L and 316L, Ti-6Al-4V, W, and ceramic materials such as Al_2O_3, ZrO_2, etc. There is also a separate problem of the spheroidization of powders used in three-dimensional (3D) printing processes using selective laser melting, electron beam melting, laser direct energy deposition, plasma metal deposition, etc. in order to improve the shape and, in some cases, to refine the chemical composition for their reuse in additive manufacturing [1,5,7,11,12]. In addition, there is a significant need for spherical powders for gas-thermal spraying of functional coatings, mainly by supersonic gas-flame, atmospheric plasma, and cold gas-dynamic (cold spray) spraying methods, where the density and adhesive and cohesive strength of the sprayed layers depend on the stability of powder feeding [8,10]. Another area of application of spherical powders is producing parts via powder metallurgy methods. Given the wide range of applications, the morphology of powder particles is one of the key factors determining the stability and efficiency of technological processes using them. The shape of the particles directly affects the flowability, uniformity of feeding, and density of powder spraying, pressing, or layer-by-layer deposition in additive manufacturing [13]. In this context, spherical powders provide a number of fundamental advantages compared with irregular ones. Due to the minimal coefficient of friction and the absence of mechanical adhesion between the particles, they are characterized by improved fluidity and uniformity of supply to the spraying or melting zone [3,7]. In addition, the high bulk density and compact packing of particles contribute to the formation of homogeneous layers with smaller gaps, which increases the density and reduces the porosity of the final products. The spherical shape also provides more uniform heat absorption by particles during plasma or laser heating, which allows for more complete melting of the material and stable formation of the microstructure of the coating or part [7]. As a result, coatings and products manufactured using spherical powders are characterized by higher cohesive and adhesive strength, improved mechanical and performance properties, and increased reproducibility of the results compared with powders of an irregular shape [1,4]. That is why increasing the sphericity of powder materials is considered as one of the key areas for improving the technological processes of plasma spraying, 3D printing, and powder metallurgy [14].

Currently, plasma spheroidization of irregularly shaped powders is carried out using radio-frequency inductively coupled plasma (RF-ICP), microwave plasma, and in arc-discharge plasma (mainly direct current) [15–17].

RF-ICP is generated by inducing an electromotive force in the gas under the action of an alternating magnetic field created by a coil through which a high-frequency current flows (the frequency usually ranges from 0.45–13.56 MHz). Microwave plasma is generated using microwave

fields in the frequency range from 300 MHz to 300 GHz. Ionization occurs without electrodes, due to the energy transferred to the electrons from the oscillating electromagnetic field. The temperature of the RF-ICP is usually 6,000–10,000 K (gas temperature), and the electron density is up to 10^{15} cm^{-3} [18,19]. These values are lower than those of arc plasma, but RF-ICP is characterized by high purity, stability, and no electrode erosion. The RF-ICP method has also become widespread in the processes of spheroidizing irregularly shaped powders due to the lower velocity of the plasma jet and, accordingly, the significant residence time of the powder in the processed medium, a high degree of ionization, and the plasma temperature. This method allows for the effective spheroidization of both metal and ceramic powders with a sphericity coefficient close to 0.90–0.95 [17]. However, the efficiency of RF-ICP and microwave plasma torches usually does not exceed η = 40%–60% [20,21], and the cost of such equipment is significantly higher compared with direct current arc systems. This is due to the high price of high-frequency generators and matching units, and the lower prevalence of such systems in industrial production. In contrast, the manufacturing of arc plasma torches is well standardized and is characterized by significantly higher availability.

Arc plasma is formed by a direct electric discharge between the cathode and the anode, through which a high-density electric current (up to 10^6 A/m^2) passes. Energy is supplied directly to the ionized medium due to electron ion conductivity, so the plasma has a high temperature (up to 25,000–30,000 K) and a significant electron density (10^{16}–10^{18} cm^{-3}) [22]. The arc discharge used to generate high-temperature plasma can exist in two main varieties—direct current (DC) and alternating current (AC). However, alternating current plasma torches have not gained wide practical application due to a number of technological limitations [23]. In particular, periodic current crossing through zero leads to the arc extinguishing and reigniting, which causes temperature fluctuations, instability in the plasma jet, increased electrode erosion, and a decrease in thermal efficiency. In addition, due to the cyclic change in the electrode's polarity, there is a decrease in the service life of cathode–anode assemblies and the difficulty of maintaining a stable anode–cathode discharge [24].

In this regard, plasma spheroidization of irregularly shaped powders in arc plasma is carried out using DC plasma torches, which are used for various technological processes in material processing [25–27]. The use of such plasma torches allows users to obtain stable plasma jets with high enthalpy and controlled energy characteristics, where the electric power can reach 250 kW and more [28,29]. Due to this, this method can provide uniform heating and melting of particles in the plasma jet, which contributes to the formation of a spherical shape even in nonmetallic materials with a high melting point, low thermal conductivity, and high heat capacity, such as oxides, carbides, and nitrides, etc [30–32].

The purpose of work is to analyze modern designs of DC plasma torches and the effectiveness of their application for spheroidization processes of irregularly shaped powders.

To achieve this goal, the following tasks are undertaken in the article:

1. To analyze the existing designs of DC plasma torches and identify the most promising types for the processes of spheroidization of irregularly shaped powders, taking energy efficiency, arc stability, and electrode life into account.

2. To perform a theoretical analysis of the physical features of the DC plasma arc as a source of thermal energy and the processes of its interaction with the dispersed material from the point of view of the influence of the processing parameters on the degree of melting of powder particles and the formation of their spherical morphology.

3. To substantiate modern design and technological approaches to the implementation of the plasma spheroidization process, aimed at increasing productivity and the quality of spheroidized powder and expanding the possibilities of the industrial use of DC plasma torches.

2. Classification of DC plasma torch designs used for plasma spheroidization of irregularly shaped powders

It is known that currently the most common designs of plasma torches (Figure 1), which are used for the spheroidization of irregularly shaped powders, are single-electrode designs with one cathode and anode (Figure 2), which operate mainly at currents of 500–800 A [33].

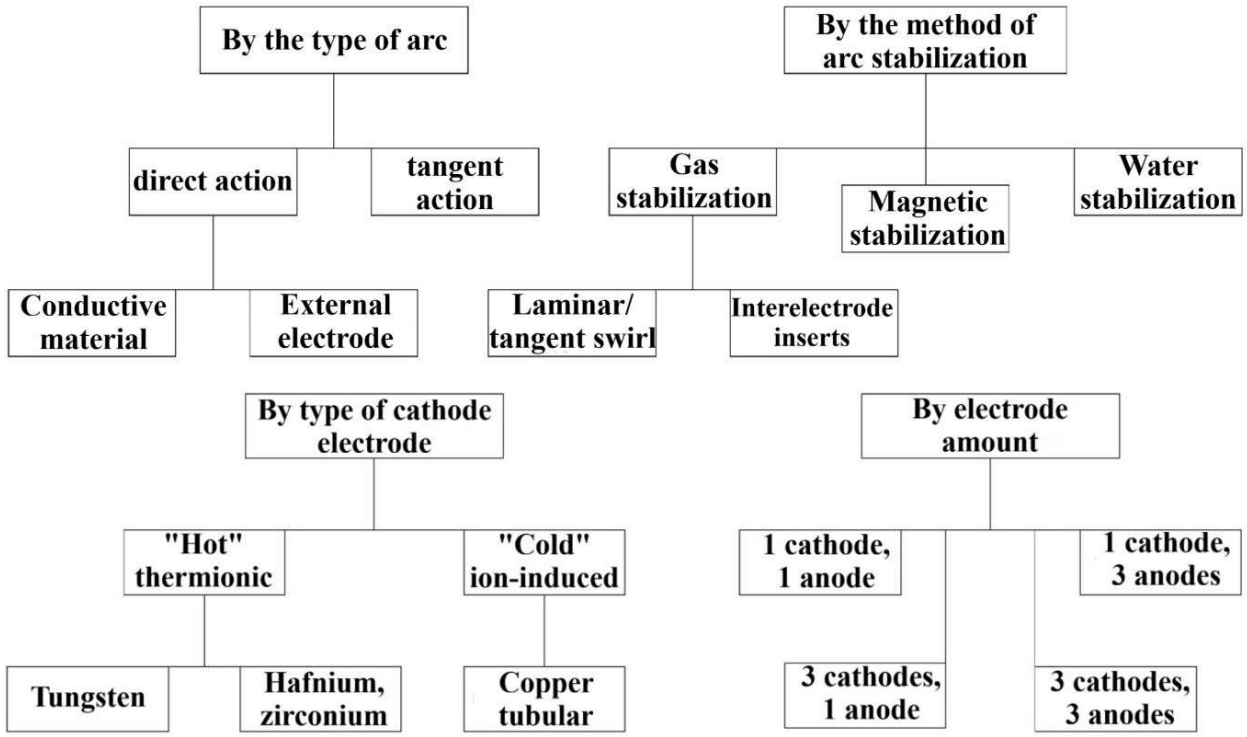

Figure 1. Classification of DC plasma torches.

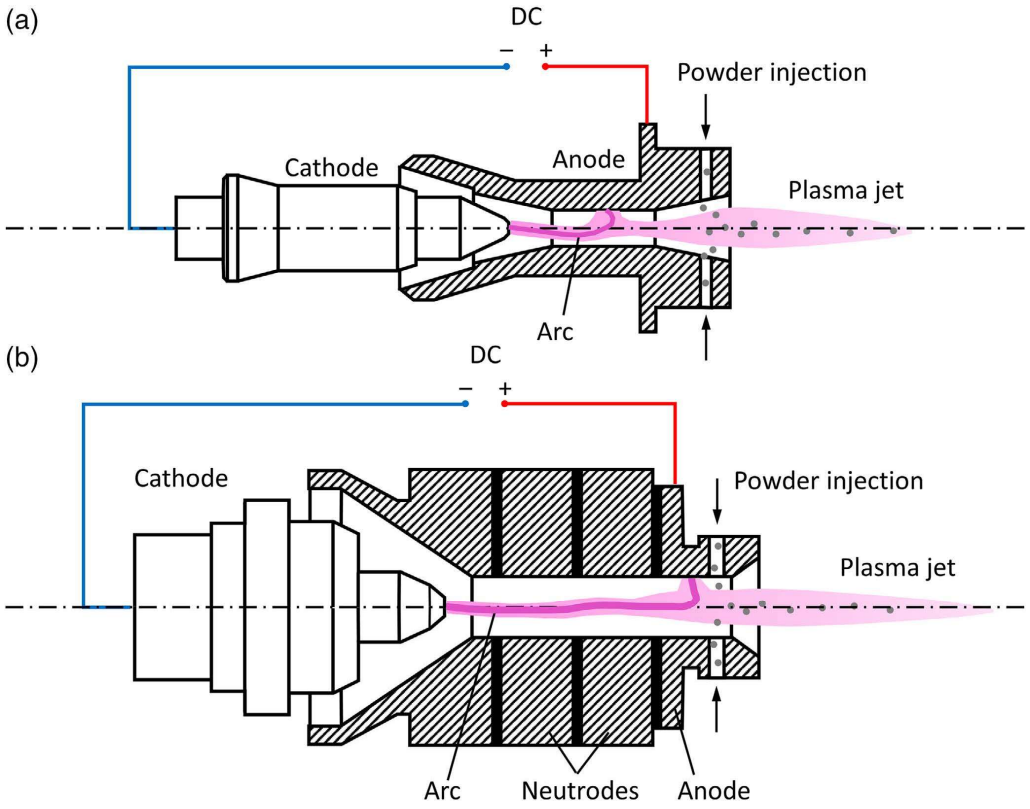

Figure 2. Scheme of single-electrode designs of plasma torches for plasma arc spheroidization of irregularly shaped powder with a "hot" tungsten cathode (a) without and (b) with an interelectrode insert (cascade system) (Reproduced from Ref. [34] with permission).

Plasma torches of this design include the 3MB, F4, and SinplexPro models (Oerlikon Metco, Switzerland) with a power of up to 60 kW, and SG 100 (Flame Spray Technologies, Netherlands), with a power of up to 80 kW. At the same time, the main components of the plasma torch, namely the electrodes, which largely determine the service life and reliability of its operation, are prone to "aging" and wear (Figure 3), especially when operating at currents usually exceeding 400 A [35].

One of the reasons for this phenomenon is the high current densities, which can reach values of 1×10^8 A/m^2, especially in the cathode spot zone when using tungsten thermionic cathodes [35,37]. In addition, electrode wear leads to significant arc oscillations (fluctuations) within ±20 V, which worsens its dynamics [36]. As a result, these plasma jet pulsations affect the stability of the process, while the uniformity of the distribution of axial and radial gradients of velocity and the temperature of the plasma jet deteriorates [38,39], which leads to uneven melting of the powder introduced into the plasma jet.

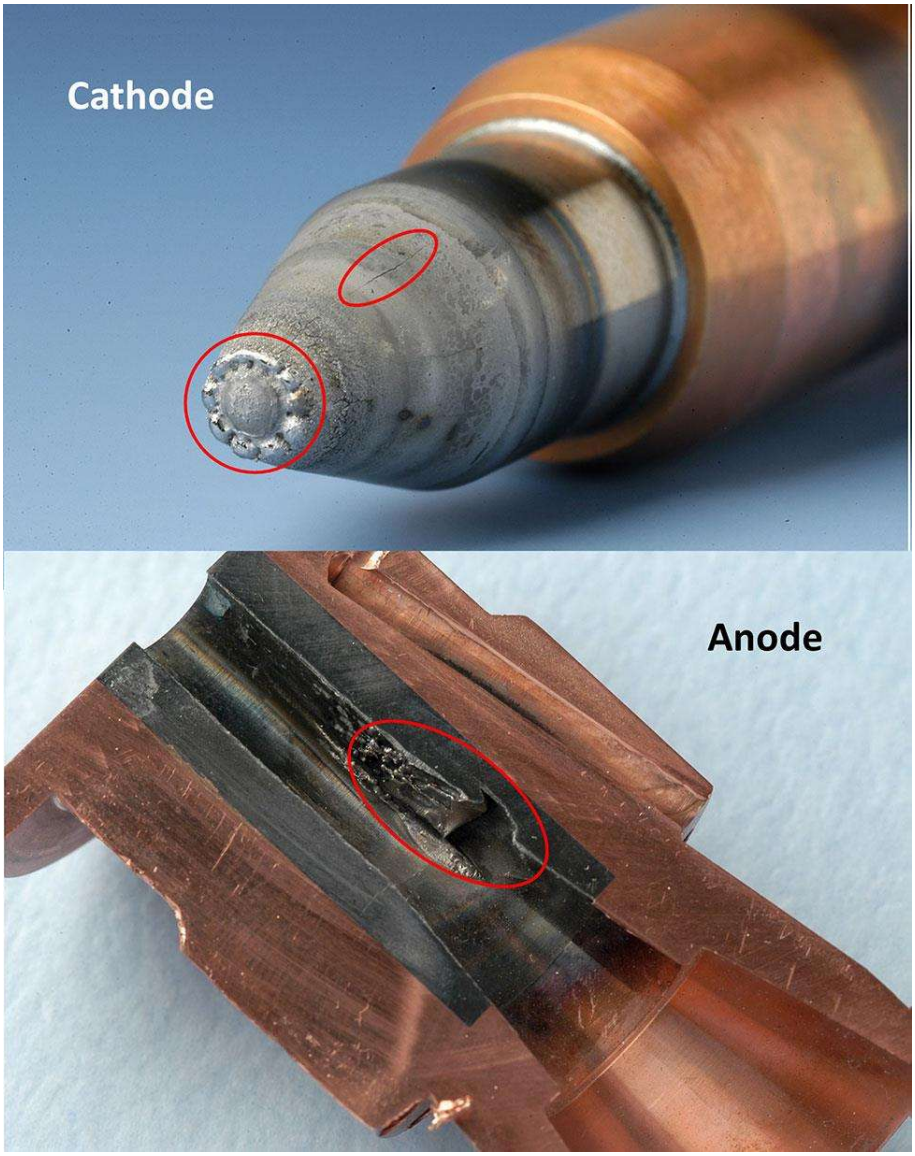

Figure 3. Worn cathode (top) and anode (bottom, cross-section) of a traditional single cathode–anode F4 plasma torch (Reproduced from Ref. [36] with permission).

Currently, the intensive wear of electrodes, which causes arc fluctuations and power fluctuations, has become the starting point for the development of new concepts of high-power plasma torches, such as multi-electrode (Figure 4a,c) and/or cascade systems (Figure 4b), where the arc fluctuations do not exceed ±5 V [40–43]. Such promising plasma torch models include TriplexPro 210 (Oerlikon Metco, Switzerland). with a power of up to 65 kW; Delta (GTV, Germany), with a power of up to 75 kW; and Axial III (Mettech, Canada), with a power of up to 100 kW.

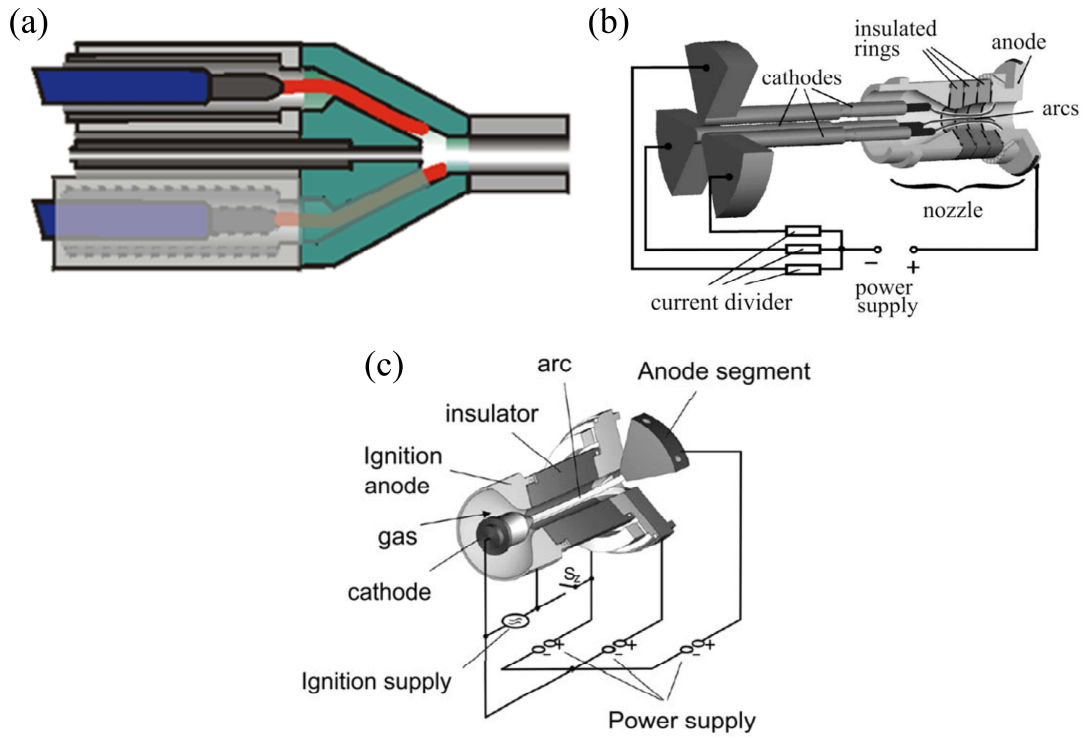

Figure 4. Scheme of multi-electrode designs of plasma torch for plasma arc spheroidization of irregularly shaped powder with a "hot" tungsten cathode: (a) three cathodes, one anode (Axial III, Mettech); (b) three cathodes, one cascade anode (TriplexPro 210, Oerlicon Metco); (c) one cathode, three anodes (Delta, GTV) (Reproduced from Ref. [44] with permission).

Such plasma torches are characterized by increased stability of operation and increased service life, since the use of a multi-cathode system contributes to a decrease in the current density in each of them with a constant total arc power [45], and the use of a cascade system allows for effective limitation of axial movements of the anode spot [46]; as a result, the arc's behavior becomes more stable (voltage fluctuations can be up to 1%), and the output power is practically unchanged during operation [39,40].

However, the design of such plasma torches is very complex and requires significant technological and material resources for its implementation and manufacture. Also, a significant drawback of both single-cathode and multi-cathode systems with thermionic "hot" tungsten cathodes is the need to operate only in inert environments of monatomic gases of argon and helium, where the amount of additional (polyatomic) gas, which can significantly increase the enthalpy of the plasma jet (nitrogen, hydrogen, methane, oxygen, etc.) [47,48] cannot exceed 5%–10%, since this leads to intensive erosion of the tungsten cathode [35].

It has been experimentally found that at a cathode temperature close to the melting point of tungsten when using nitrogen as a plasma-forming gas, the excess thermionic emission current density is more than one order of magnitude (j_{exp} = (3–6) × 10^8 A/m^2 [49] compared with the thermionic emission current density, accounting for the specified cathode temperature T_c and the correction for the Schottky effect when using argon as the plasma-forming gas [50], which, in turn, leads to intensive evaporation of atoms from the cathode's surface j_{em}^{TE} (Eq 1):

$$j_{em}^{TE} = j_{em}^{T}\exp\left(\frac{\sqrt{q_e^3 E_c/\varepsilon_0}}{k_B T_C}\right) = 3 \times 10^7 A/m^2 \quad (1)$$

Theoretical studies of the process of atom evaporation from the surface of a tungsten cathode during plasma sputtering, performed in [51], showed that a certain fraction of evaporated atoms can return to the cathode in the form of ions, reducing the flux of evaporated atoms J_{vap} (Eq 2) compared with the value given by the Langmuir equation.

$$J_{vap} = \frac{p_v}{\sqrt{2\pi m_w k_B T_c}} \quad (2)$$

To estimate the number of evaporated atoms that do not return to the cathode, the following analytical model (Eq 3) was proposed in [52]. According to this model, tungsten atoms are instantly ionized and diffused in the plasma, with further intensification of this process when polyatomic gases of nitrogen, hydrogen, methane, etc. are added to argon.

$$\frac{G}{G_0} = \frac{J_i}{3e\overline{v}_{Ar}N_{e,\infty}^2 L_{ion} S_c} \times \sqrt{\frac{M_w}{M_{Ar}}} \times \left[\int_0^{\zeta_b} \eta^2(\varsigma)d\varsigma\right]^{-1} \quad (3)$$

Due to the fact that only a small portion of the evaporated material re-deposits on the cathode, a significant amount leaves the cathode region and enters the arc column, where it typically deposits on the cold peripheral surface of the cathode and on the inner walls of the plasma torch discharge chamber, which are intensively water-cooled [53]. Experimental studies determining the erosion intensity of tungsten cathode material have shown that in the current range of 600–800 A, when using single-electrode plasma torches of the F4MB type and argon as the plasma-forming gas, the erosion intensity reaches up to 1.1×10^{-12} kg/C, while the use of nitrogen as the plasma-forming gas at currents up to 400 A leads to a fivefold increase in the tungsten cathode's erosion intensity to approximately 5×10^{-12} kg/C [49].

Thus, intensive cathode erosion when using di- and polyatomic gases such as nitrogen, oxygen, hydrogen, methane, etc. is due to an abnormally high density of thermionic currents [49]. Under such conditions, one of the possible methods of reducing cathode erosion is local purging of the tungsten cathode's surface with a small amount of inert gas (argon), with subsequent passage of the main gas flow (N_2, H_2, CH_4, etc.) through the plasma. This approach allows one to create a protective shell around the cathode spot, reduce the temperature of local overheating, and, accordingly, the intensity of tungsten evaporation.

Another solution is the replacement of "hot" tungsten cathodes with "cold" copper (tubular) ones, which reduces electrode wear and expands the range of plasma-forming gases. The concept of low-current (up to 200 A) and relatively high-voltage (up to 1000 V) plasma torch designs provides lower erosion of the cathode and anode [54], longer service life, and practically no contamination of the dispersed material (powder, coatings, etc.) by the products of electrode erosion [55–58]. An interesting design is that of plasma torches with tubular copper inner electrodes, one of which has a blind axial hole, operating under reverse polarity (Figure 5), where the plasma-forming copper nozzle acts as the cathode and another copper electrode with a through-hole acts as the anode. Plasma-forming gases may include both monoatomic gases such as argon and helium, as well as polyatomic gases such as nitrogen, hydrogen, methane, and others, as well as their mixtures, which allows the formation

of high-enthalpy plasma jets at relatively low current loads (including up to 100 A) on the inner electrodes [59–61].

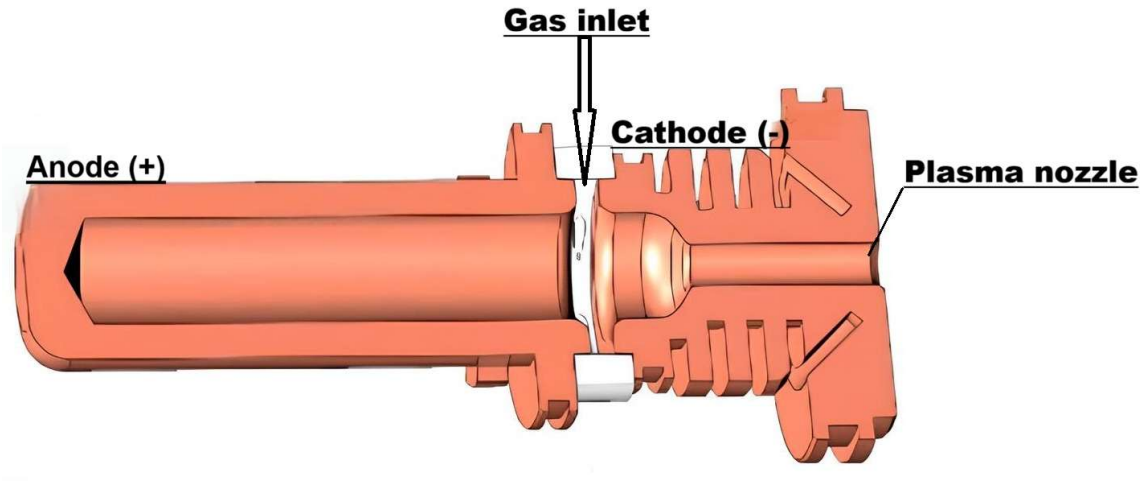

Figure 5. 3D model of a plasma torch with tubular copper inner electrode.

In previous work [61], it was shown that the erosion intensity of the tubular copper cathode in the abovementioned plasma torches can reach up to 1×10^{-14} kg/C at a plasma torch power of 40 kW. Thus, the application of the low-current and relatively high-voltage plasma torch design concept with tubular copper electrodes first ensures lower electrode erosion and practically eliminates contamination of the processed material by the products of electrode erosion and, second, makes it possible to increase the efficiency of processing dispersed material in the plasma jet through the use of different types of plasma-forming gas mixtures.

3. Basic physical principles of the process of spheroidizing irregularly shaped powder in low-temperature plasma generated by DC plasma torches

The essence of the process of spheroidizing irregularly shaped powders using DC plasma torches is the effect of a high-enthalpy plasma jet on powder particles, with the aim of their partial or complete melting (Figure 6a). Under the influence of surface tension forces, the molten particles tend to minimize the free energy of the surface, taking a shape close to spherical [62]. After leaving the high-temperature zone, they undergo rapid cooling and solidification, which fixes the spherical shape of the particle. The stages of the plasma spheroidization process are described below (Figure 6b).

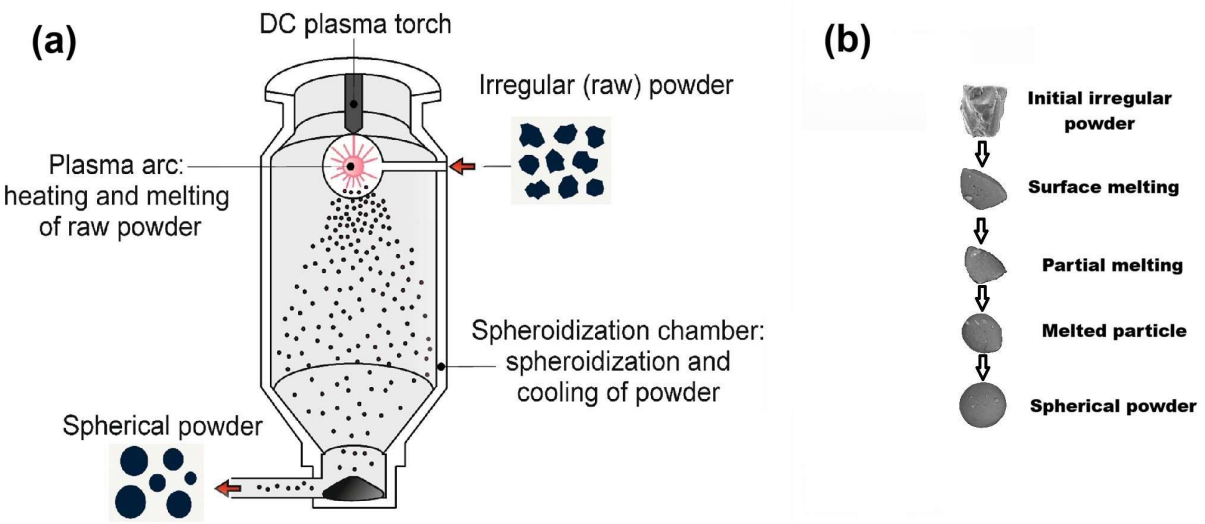

Figure 6. (a) Scheme and (b) stages of the process of plasma spheroidization of irregularly shaped powder using DC plasma torches.

3.1. Injection of powder into the plasma jet

Powder particles are fed into the high-temperature jet region either radially [63] or axially [64]. Currently, the most common scheme for injecting powder into the plasma spheroidization process is the radial scheme (Figure 7a). This scheme involves feeding the powder into the plasma jet in a direction perpendicular to its outflow axis.

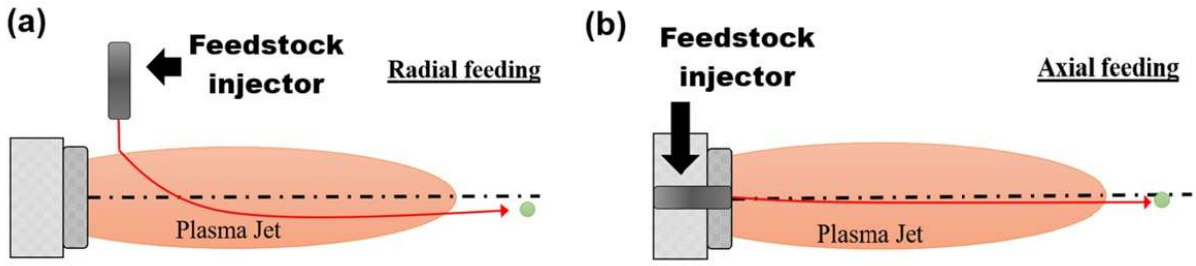

Figure 7. (a) Radial and (b) axial scheme of feeding powder into the plasma jet (Reproduced from Ref. [65] with permission).

The main advantage of this scheme compared with axial powder injection (Figure 7b) is its simplicity of implementation, which is due to the simplified design of the plasma torch's gas discharge chamber and the absence of the need for complex internal channels for supplying powder through the electrode or the central zone of the plasma torch. This approach simplifies the cooling system, reduces the erosion load on the internal parts, and reduces the cost of manufacturing the plasma torch, etc. However, despite the design advantages, radial injection is significantly inferior to axial injection in terms of the efficiency of heating the powder material introduced into the plasma jet [65]. With radial injection, powder particles cross the jet transversely and spend a limited time in the high-temperature zone, which leads to uneven heating, incomplete melting, and lower sphericity of the resulting powder.

Theoretical studies of the kinetic conditions of radial feeding of powder into the plasma jet during plasma spheroidization of irregularly shaped Al_2O_3 powder [66], performed by solving the system of Stokes equations (Eq 4), showed that depending on the force *F* acting on the particle fed into the plasma jet and depending on the magnitude of this force, it can introduce particle into its central or peripheral zone:

$$F = 6\pi \times Q \times \nu \times r \times V \tag{4}$$

where υ is the coefficient of kinematic viscosity of the plasma, *V* is the velocity of the particle in the direction perpendicular to the movement of the plasma jet, *r* is the radius of the particle, and *Q* is the flow rate of the plasma-forming gas.

At the same time, experimental studies have shown that at the optimal flow rate of plasma-forming gas for a certain narrow fraction of powder, the exposure of particles into the central zone of the plasma jet, compared with the exposure into the peripheral zone, increases the degree of spheroidization of the powder by 30%–40%.

During the flight, several forces act on the particle: the thermophoresis force, the Coriolis force, and others [67–69]. Theoretical studies of the motion of particles in a plasma jet [70,71] have shown that the greatest influence on the particle is exerted by the aerodynamic drag force. The velocity of a particle of arbitrary shape along the flight distance can be determined from Eqs 5–7:

$$\mathrm{m_p W_p} \frac{\mathrm{dW_p}}{\mathrm{dz}} = 0.5\mathrm{C_D S_p \rho_g (W_g - W_p)\left|W_g - W_p\right|} \tag{5}$$

where m_p and W_p are the mass and velocity of the particle, respectively; C_D is the drag coefficient; S_p is the average cross-sectional area of the particle; and ρ_g and W_g are the density and velocity of the gas, respectively.

The motion of a spherical particle in a plasma jet [72] can be described by the Eq 6:

$$\rho_p \frac{Dv_P}{dt} = C_D \frac{3\rho_s (v_s - v_p)^2}{4D_p} \tag{6}$$

where ρ_p, v_p, and D_p are the density, velocity, and diameter of the particle; ρ_s and v_s are the density and velocity of the plasma jet; *t* is the time the particle spends in the plasma jet; and C_D is the drag coefficient.

It is known that the main difficulty in calculating the velocity of a particle in a plasma jet is associated with the uncertainty of the values of the coefficient C_D in the plasma jet.

In [73], Eq 7 was proposed by which one can find the relationship between the coefficients of aerodynamic resistance and the sphericity of particles:

$$C_D = \frac{24}{Re}[1 + 8.1716\exp(-0.40655Ø)]Re^{0.0964+0.5565Ø} + \frac{73.69Re\exp(-5.748Ø)}{Re+5.378\exp(6.2122Ø)} \tag{7}$$

where *Re* is the Reynolds criterion and *Ø* is the sphericity coefficient of the powder.

Analyses of theoretical models of particle motion in a plasma jet from the point of view of spheroidizing irregularly shaped powders showed that the most effective is the axial powder feed scheme. It provides the introduction of particles directly into the central high-temperature zone of the jet, where the maximum level of thermal impact is realized, which contributes to intensive melting and the formation of a spherical morphology. To increase the degree of spheroidization, it is advisable to increase the residence time of particles in the plasma jet, which can be achieved by reducing the

velocity of the gas–powder mixture or using longer plasma jets with increased enthalpy. In the case of radial feed, the efficiency of the process largely depends on the dimensional uniformity of the material: it is necessary to use narrow powder fractions and select a flow rate of the transport gas in such a way that the trajectories of particle motion are focused in the central part of the plasma jet, where a sufficient level of thermal exposure is provided.

3.2. Heating and melting of powder in a plasma jet

When the powder enters the plasma jet, the individual particles are heated by thermal conduction and convection (Q_{cv}) (Eq 8), while they lose energy through radiation, Q_r (Eq 9) [74].

$$\mathrm{Q_{cv}} = h(\mathrm{T_\infty} - \mathrm{T_s}) \tag{8}$$

$$\mathrm{Q_r} = \varepsilon\sigma(\mathrm{T_s^4} - \mathrm{T_w^4}) \tag{9}$$

where h is the heat transfer coefficient, T_∞ is the plasma temperature, T_s is the particle surface temperature, ε is the particle emissivity, and σ is the Stefan–Boltzmann constant.

For complete melting of the particles, the energy obtained by the particles during their motion in the plasma jet Q_{net} (Eqs 10 and 11), which is the integral of the net energy obtained during their stay in the plasma, must be higher than the energy required to heat the particles to their melting point, the latent energy of melting, and a certain degree of superheating:

$$\mathrm{Q_{net}} = \mathrm{Q_{cv}} - \mathrm{Q_r} \tag{10}$$

$$\int_0^\tau \mathrm{Q_{net}} > \mathrm{mc_p}(\mathrm{T_m} - \mathrm{T_\infty}) + \mathrm{mH_m} + \mathrm{mc_p}(\mathrm{T_s} - \mathrm{T_m}) \tag{11}$$

where m is the mass of the particle, c_p is the specific heat of the particle, T_m is the melting point of the particle, T_∞ is the plasma temperature, H_m is the latent heat of fusion of the particle, s is the surface temperature of the particle, and τ is the residence time of the particle in the plasma jet.

In [75], Eq 12 was proposed to calculate the thermal power that must be transferred to the particles for their spheroidization:

$$\mathrm{N_G} = \mathrm{G_p} \cdot \left[\int_{\mathrm{T_0}}^{\mathrm{T_m}} \mathrm{c_{pm}} \cdot \mathrm{dT} + \mathrm{Q_m} + \int_{\mathrm{T_m}}^{\mathrm{T_b}} \mathrm{c_{pl}} \cdot \mathrm{dT} + \left(\mathrm{Q_v} + \int_{\mathrm{T_b}}^{\mathrm{T_v}} \mathrm{c_{pv}} + \mathrm{J} \cdot \mathrm{Q_+}\right)\right] \cdot \left(1 - \frac{\mathrm{r_p^3}}{\mathrm{r_{p0}^3}}\right) \tag{12}$$

where G_p is the mass flow rate of the powder, T_m is the melting point of the material, c_{pm} is the specific heat of the material in the solid state, Q_m is the specific heat of fusion, c_{pl} is the specific heat of the material in the liquid state, T_b is the boiling point of the material, Q_v is the specific heat of vaporization of the material, c_{pv} is the specific heat of the material in the vapor state, T_v is the ionization temperature of the material, J is the degree of ionization, and Q_+ is the specific heat of formation of a singly ionized vapor.

Moreover, an important characteristic of the process under consideration is the time of heating the particle surface to the melting temperature, the calculations of which can be carried out using Eq 13 [76,77]:

$$\mathrm{t_m} = \frac{\mathrm{r\lambda}}{3\alpha} \ln \frac{(\mathrm{T_g} - \mathrm{T_0})}{\mathrm{T_g} - \mathrm{T_m}} \tag{13}$$

Theoretical analysis of the mechanisms of heat exchange between the plasma and the particles injected into it showed that for complete melting of the particles, it is necessary to ensure that the integral heat obtained during their stay in the plasma jet exceeds the total energy consumption for heating to the melting point, the latent heat of fusion, and subsequent overheating of the melt. This requires optimization of both the plasma torch's parameters (temperature and enthalpy of the plasma jet) and the parameters of powder injection (mass, size distribution, speed, and duration of stay in the torch). The time of heating the particles to the melting temperature is also of practical importance, which depends on their size and thermophysical properties. An increase in the particle size significantly increases the time to reach the melting temperature, which complicates complete spheroidization. In addition, the heating efficiency significantly depends on the choice of plasma-forming gas. The use of gases with high thermal conductivity and enthalpy (helium, nitrogen, hydrogen, air, and methane) promotes more intense heat transfer to the surface of the particles, reduces their heating time, and expands the range of sizes suitable for spheroidization.

3.3. Formation of a spherical particle shape

In the molten state, surface tension forces smooth out irregularities and angles, bringing the particle to the minimum free energy of the surface—a sphere. At this stage, uniformity of heating and a sufficient duration of the particles' stay in the high-temperature zone are important.

Theoretical calculations given in [78] showed that an increase in the degree of superheating of the liquid metal (particles) leads to a decrease in the surface tension force, while the kinetic energy of atoms increases, interatomic bonds at the liquid–gas interface weaken, and the energy required for the formation of a new surface decreases, which facilitates the formation of drops of a regular shape and promotes the process of their spheroidization. The surface tension force of a drop (Eq 14) is determined as a function of temperature [79]:

$$\sigma = \sigma_m - k(T - T_m) \tag{14}$$

where σ_m is the surface tension force of the particle at the melting temperature T_m and k is the temperature coefficient of the material.

Mikhalev and Petrunichev [80] believe that the residence time of the powder in the plasma jet t is the limiting factor of the spheroidization process and can be determined from Eq 15:

$$\mathrm{t} = \sqrt{\frac{2S}{AV_g}}, \mathrm{A} = \frac{4.5\eta}{r^2\rho} \tag{15}$$

Another formula for determining the time required for the spheroidization of powder was proposed in [81], as Eq 16:

$$\tau_{sph} = \frac{1.785\pi \cdot r_k \cdot \mu_m}{\sigma_m} \tag{16}$$

where r_k is the radius of the particle after its solidification, μ_m is the dynamic viscosity of the molten particle, and σ_m is the surface tension coefficient of the metal.

In [82], Eq 17 was proposed, which can be used to determine the criterion B, which characterizes the intensity of the spheroidizing effect of plasma on powder particles:

$$B = \frac{t}{t_m} = \frac{2\alpha\sqrt{S/(\eta\rho_g)}}{c_p \ln\left[2\left(T_g - T_0/(T_g - T_m)\right)\right]} \quad (17)$$

Thus, a spheroidization criterion value of $B \geq 0.8$ corresponds to a yield of spherical particles greater than 60%.

Analysis of the equations above for determining the residence time of the powder in the plasma jet showed that for effective spheroidization of particles, it is necessary to ensure conditions of uniform heating and sufficient residence time in the central high-temperature zones of the plasma jet [83–85]. In this case, increasing the degree of overheating of the molten particles by increasing the power of the plasma torch and the enthalpy of the plasma jet reduces the surface tension force, which facilitates the formation of the spherical shape of the droplets and contributes to an increase in the proportion of spherical granules in the final product. At the same time, the residence time in the torch acts as a limiting factor to ensure a spheroidization efficiency of 95%–100%. It is necessary to select the feed parameters and gas flow rate so that the particles pass through the hottest parts of the jet. In addition, increasing the length of the plasma jet contributes to the lengthening of the trajectory of particle motion in the high-temperature zone, which increases their residence time in the plasma and, accordingly, increases the efficiency of the spheroidization process.

3.4. Cooling and solidification of the powder

Upon exiting the hot zone, the particles cool down rapidly by heat exchange with the plasma and surrounding gas. Rapid quenching fixes the spherical shape and can lead to the formation of a fine dendritic structure or amorphous areas, depending on the material and cooling regime.

The analytical equation that can be used to calculate the time required for the particles to solidify after passing through the plasma jet is as Eq 18 [77,81]:

$$\tau_s = \frac{c_m \cdot \rho_p \cdot d_k}{6\alpha} \ln \frac{t_m - t_g}{t_{mel} - t_g} \quad (18)$$

where c_m is the specific heat capacity of the metal, t_m is the temperature of the metal, t_g is the temperature of the gas, t_{mel} is the crystallization temperature of the metal, and α is the heat transfer coefficient for the final drop.

Theoretical analysis of the equations above showed that for reliable fixation of the spherical shape of particles, especially in the case of materials with low thermal conductivity (particularly ceramics), solidification of the particles must occur before the particles collide with the walls of the receiving chamber (powder collection hopper). Otherwise, their deformation and deterioration of their spherical shape are possible.

4. Technological schemes of the spheroidization process of irregularly shaped powders using DC plasma torches

Studies have been devoted to the spheroidization of ceramic powder of Al_2O_3 (Figure 8a,b) and stainless steel SS316L (Figure 8c,d) with particle sizes of –25 and –45 μm, respectively, at a plasma torch power of 18–43 kW [86,87]. They found that radial powder feeding when using single-electrode

conventional plasma torches (Figure 2a) in the general case provides no more than 70–80 wt.% of spheroidized powder. In addition, the productivity of the process with such a spheroidization scheme does not exceed 2–17 g/min.

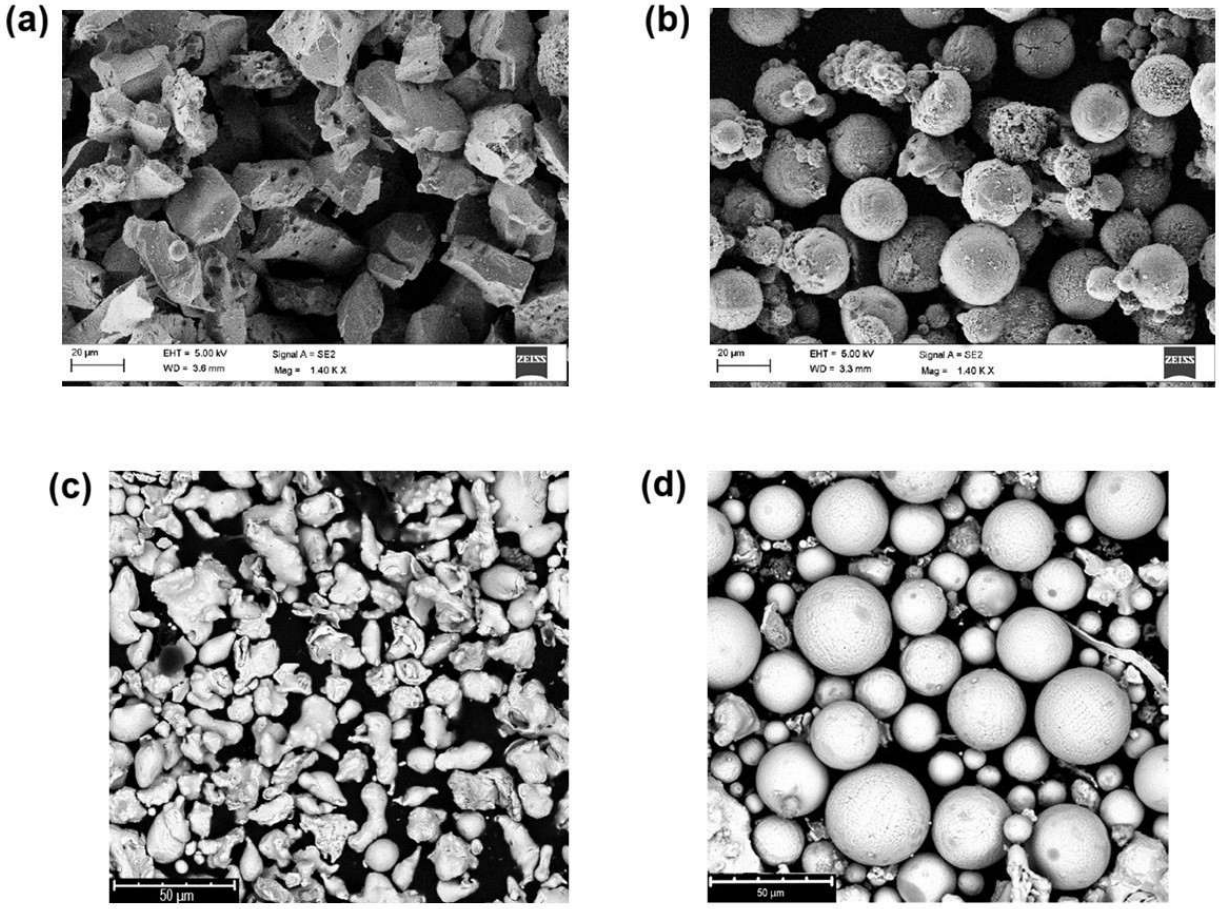

Figure 8. (a) Scheme of the F4MB-XL plasma torch with a single cathode–anode and radial powder feed into the plasma jet. Appearance of the powder (b, d) before and (c, e) after spheroidization process. (b, c) Al_2O_3 fraction, –25 μm; (d, e) stainless steel SS316L fraction, –45 μm (Reproduced from Ref. [86,87] with permission).

In one study [88], the efficiency of the spheroidization of oxide powders (Zr_2O_3–7YSZ and Al_2O_3) with a particle size of 40–120 μm was investigated in a nitrogen plasma jet with the addition of a combustible gas (methane), using a cascade-type plasma torch and radial injection of the powder into the plasma jet from four points. It is noted that nitrogen plasma at a plasma torch power of 50–75 kW enables effective spheroidization of the initial irregularly shaped powders (Figure 9), produced by spray-drying technology, while the process's throughput can reach 20 kg/h. This is attributed, on the one hand, to the higher enthalpy of nitrogen plasma, which, in the temperature range of 10,000–20,000 K, reaches 50–175 kJ/kg, compared with argon plasma, where the enthalpy does not exceed 5–30 kJ/kg [89]; on the other hand, it is attributed to the four-point powder injection method, which also significantly increases the process's productivity.

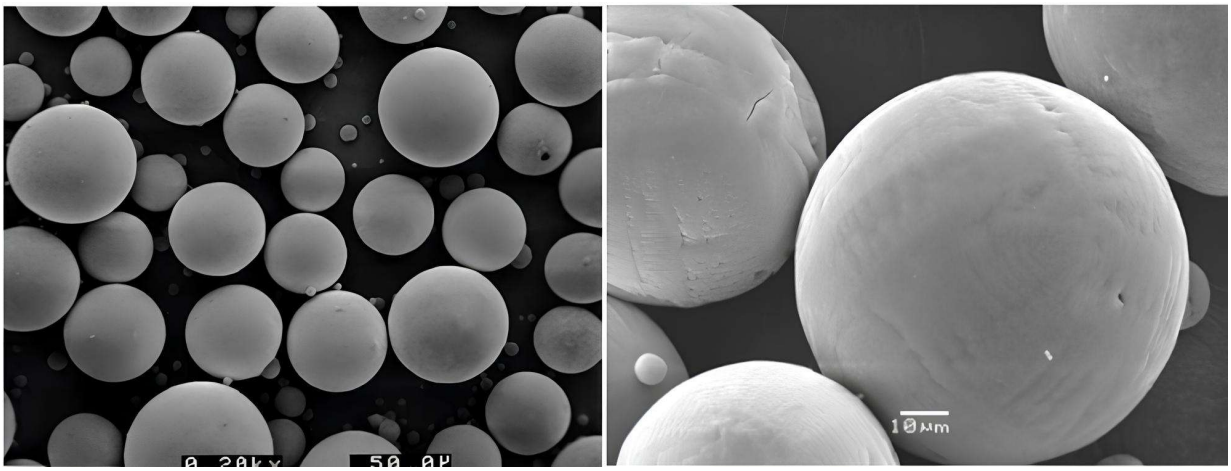

Figure 9. Appearance of spheroidized aluminum oxide powder (Al_2O_3) with a particle size of 15–45 μm after spheroidization using a cascade plasma torch (Reproduced from Ref. [88] with permission).

However, a significant disadvantage of this type of plasma torch is that it can only operate when nitrogen and air are used as the plasma-forming gases, which makes it impossible to process chemically active materials such as titanium, aluminum, zirconium, etc.

In some research [90], an example of implementing an axial scheme for feeding powder into a plasma jet using a specialized three-cathode plasma torch with a common anode (Figure 10), which is powered by three independent DC sources, is given.

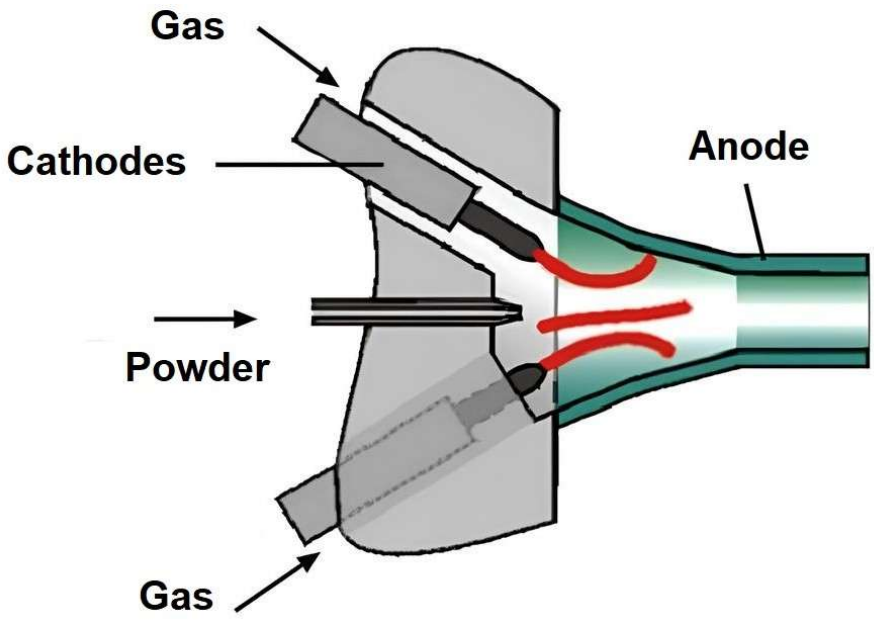

Figure 10. Scheme of the plasma torch for a three-cathode spheroidization process with axial powder feed (Reproduced from Ref. [44] with permission).

Authors investigated the influence of the nozzle-anode's geometry on the efficiency of spheroidizing stabilized zirconium oxide (ZrO_2–7YSZ) powder of the +10, –80 μm fraction [90]. By solving the

system of magnetohydrodynamics equations, the velocity and temperature characteristics of the plasma jets were determined, depending on the geometry of the nozzle part of the plasma torch, which provide a plasma jet outflow mode from subsonic to supersonic and their influence on the processes of powder spheroidization.

It was found that the highest percentage of spheroidized particles (96.6%) was obtained when using a medium-speed nozzle with a nozzle channel diameter of 17 mm, which provided an optimal balance among temperature, velocity, and length of the plasma jet (Table 1).

Table 1. Efficiency of the spheroidization process of ZrO_2–YSZ powder of the +10, –80 μm fraction using a three-cathode scheme with an axial feed.

Nozzle type	Spheroidization rate (%)	d_{10} (μm)	d_{50} (μm)	d_{90} (μm)
Without nozzle	62.5	20.83	37.63	57.01
High-speed	94.8	11.05	22.90	42.43
Intermediate-speed	96.6	26.67	53.17	82.15
Low-speed	90.8	26.21	43.31	62.71

At the same time, it should be noted that despite the use of a three-cathode system and an axial powder feed, the process's productivity remained quite low, up to 12 g/min. This may be due to difficulties in achieving a stable powder feed into the axis of the plasma jet, possible powder sticking to the inner walls of the nozzle-anode, or other design features of the system that were not disclosed in detail in the work.

A slightly different design of a multi-cathode plasma torch with an axial powder feed to the arc column is presented in [91,92]. In this device, six independent DC arc sources feed six plasma arcs formed between six lanthanated tungsten cathodes (2% La_2O_3, 6 mm in diameter) arranged in a circle and a common anode: a copper nozzle with a refractory tungsten insert and a central hole with a diameter of 20 mm.

An irregularly shaped powder is fed into the central (axial) zone of the plasma jet's outflow, which, passing through the zone of the high-temperature arc column, is heated, spheroidized, carried out through the nozzle, cooled, and solidified due to contact with the surrounding cold gas.

Experiments on spheroidization of irregularly shaped tungsten powder of the –45 μm fraction at a current of 450 A and an average voltage of 32.8–34.3 V for each of the power sources showed that the maximum degree of spheroidization of ~96% was achieved only when using the Ar–He 40/60 mixture as the plasma-forming gas and the powder feed rate was no more than 20 g/min [92].

The design disadvantages of the specified device include difficulties associated with the axial injection of powder into the arc column zone. The presence of six arcs, which are formed inside the plasma torch with significant gaps between them leads to an unstable powder supply directly into the arc column zone and a decrease in the number of processed particles. In addition, part of the powder can settle on the anode's surface and form a crust of melted particles. Further detachment of this crust as a result of the temperature and gas-dynamic effects of the plasma can lead to the formation of conglomerates, which, falling into the plasma jet, do not have time to completely melt. This, in turn, causes the appearance of a certain number of particles of irregular shape in the final product. There are also operational difficulties associated with the design of a six-cathode device, such as the need to use

six power sources instead of one, the difficulty in controlling and coordinating them to ensure a uniform current and voltage on all electrodes, the increase in costs for electrical equipment, etc.

Another approach to the spheroidization process is the scheme of radial feeding of powder into the section of the plasma arc column [93–96]. In devices of this scheme, the plasma arc burns between a tungsten cathode and a remote water-cooled copper anode (Figure 11) [94,97,98].

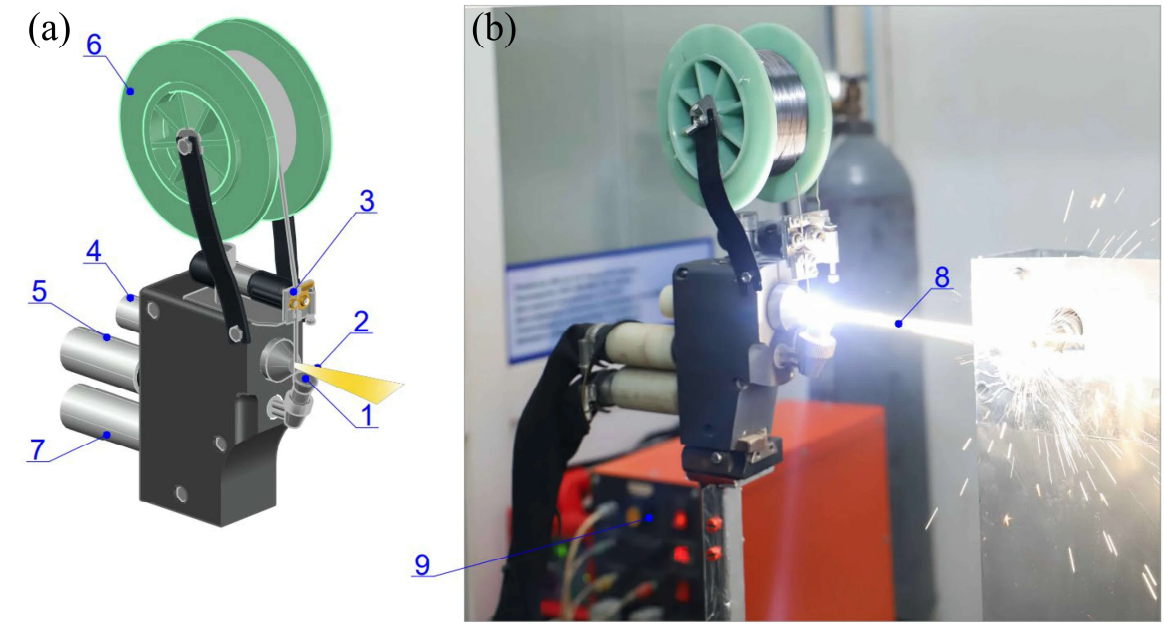

Figure 11. (a) Scheme and (b) external view of a plasma torch for microplasma spraying with radial feed of the powder or wire into the arc column. 1: Anode; 2: plasma jet; 3: wire feeding mechanism; 4: cathode; 5: plasma-forming gas supply; 6: raw material; 7: coolant and sheilding gas supply; 8: plasma arc; 9: powder supply (Reproduced from Ref. [94] with permission).

In the 1980s, equipment for microplasma spraying of coatings was developed at the E.O. Paton Institute of Electric Welding [93,99]. Metal and ceramic powders were used, which were fed into the arc column. Studies of the coatings obtained using this method [100–103] confirmed that high-density coatings were formed during the spraying process, even in the case of using a low-amperage (<50 A) arc. In [95], it was shown that with a limited plasma torch power of 3 kW, implementation of the specified powder injection scheme allows for the effective heating of ceramic powders such as stabilized zirconium oxide (ZrO_2–8YSZ) with a 40-μm fraction, while the process is characterized by indicators of quite high energy efficiency, which are ~20 kW/kg, and the thermal efficiency of the plasma torch, which can reach $\eta = 0.73$, compared with other powder injection schemes [104–106].

Another technical device of the abovementioned scheme is a plasma torch with water arc stabilization [106]. In this device, the plasma arc is also formed between a lanthanated tungsten cathode and an external copper electrode (Figure 12), the anode, which rotates [107].

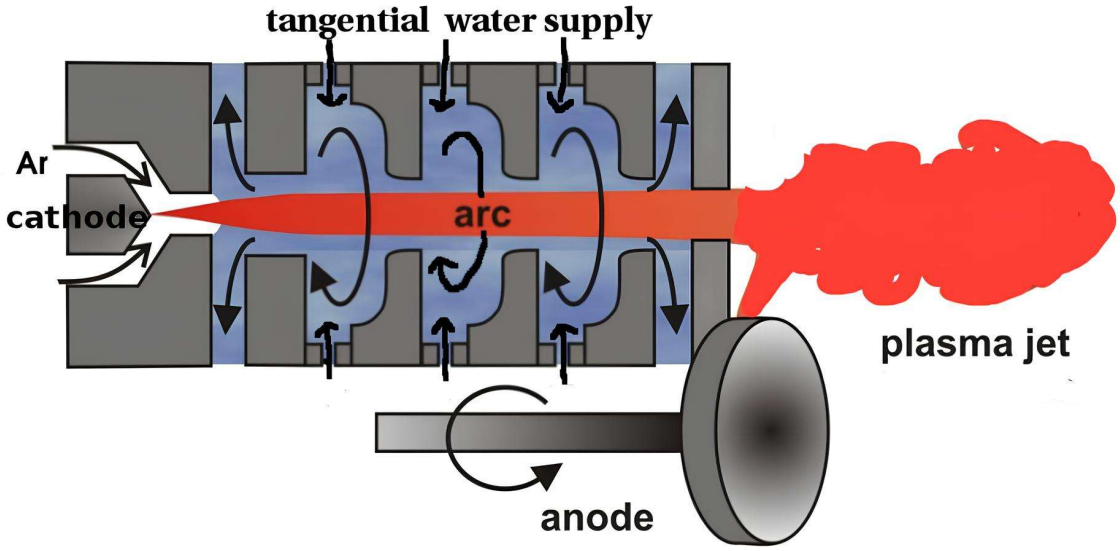

Figure 12. Scheme of the WSP®H plasma torch with a rotating copper anode (Reproduced from Ref. [107] with permission).

An experimental study of the abovementioned process [107] showed that the anode's rotation speed is ~47 m/s, while the speed of movement of the anode arc's attachment (Figure 13) along the anode's surface is 298 ± 14 m/s. This allows the operator to reduce, first of all, the electrical erosion of the external copper electrode and to operate at currents of 200–600 A, increasing the total thermal power to 200 kW.

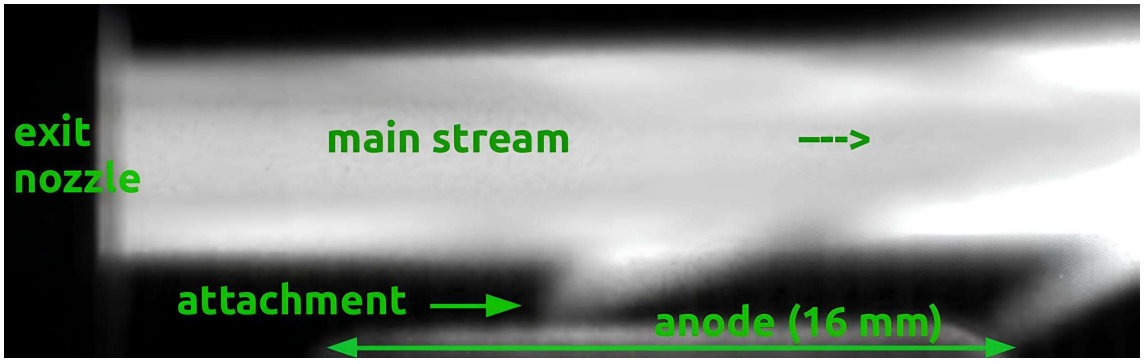

Figure 13. Location of the arc's attachment on the surface of the rotating copper anode (Reproduced from Ref. [107] with permission).

Another significant feature of the abovementioned plasma torch design is the compression of the arc column with water, which leads to an increase in the energy density, an increase in the voltage to values of 270–320 V and an increase in the arc column temperature from 16,000 to 28,000 K compared with conventional plasma torches with a power of up to 50 kW, where the stabilization of the arc discharge is carried out only by a flow of cold gas [106].

The use of a WSP®H plasma torch with an external copper electrode [108] for spheroidization of Al_2O_3 ceramic powder of the +38, –75 μm fraction can achieve productivity values of 10 kg/h with a total plasma torch power of 150 kW.

The design disadvantages of the specified device include its significant dimensions and weight due to the addition to the design of the plasma torch of a copper anode rotation unit with an asynchronous motor and a complex system for supplying coolant to the rotating anode [109]. This significantly complicates the placement of the plasma torch in vacuum chambers with a controlled atmosphere. Other drawbacks are the large dimensions of the anode unit and its fixed position, which makes it impossible to supply powder directly to the area from the end of the plasma torch's nozzle to the place of anode attachment (in the arc column), where the highest temperature of the plasma jet is diagnosed, since this will lead to powder sticking to the anode's surface. Operational disadvantages include the presence of a significant hydrogen and oxygen content in the plasma-forming gas, which, when working with such reactive metals as titanium and zirconium, leads to an increase in the hydrogen and oxygen content in the powder above permissible limits and subsequently to a decrease in the mechanical properties of products obtained using such powders.

For the task of spheroidizing powders, the design of the Axial III plasma torch (Mettech) is also of considerable interest due to its multi-cathode system and axial powder feed [110,111]. The use of three independent cathode–anode assemblies allows for the formation of a high-power torch with extended possibilities for regulating the thermal characteristics. The axial powder feed ensures the uniform introduction of particles directly into the central region of the plasma flow, which minimizes the influence of cold zones and increases the probability of complete melting of particles with an irregular shape. This makes it promising for the spheroidization of refractory materials and coarse-dispersed fractions.

At the same time, studies performed on this type of plasma torch revealed a number of features that require further study [43]. In particular, the "petal" temperature distribution of the jets, characteristic of the design associated with three arcs, leads to temporal and spatial inhomogeneity of the heating of the dispersed material (Figure 14).

Although, individual streams merge at a certain distance from the nozzle (~30 mm from the nozzle end), the question remains about the optimal length of the processing zone and the influence of plasma jet fluctuations on the stability of spheroidization (Figure 14).

It should also be noted that despite a considerable amount of research [55,57,59,61,112] on the thermal characteristics of plasma torches with tubular electrodes, there is no information regarding their application specifically in the process of spheroidization of irregular-shaped powders. The available data primarily concern their efficient use in the production of spherical powders via wire spraying technology [61,113,114].

Analyses of the thermal characteristics of DC plasma torch designs (Table 2) [115] shows that the highest efficiencies are observed in plasma torches with an external extended electrode serving as the anode (direct polarity, with the tungsten electrode acting as the cathode) and in plasma torches with tubular copper electrodes, where the efficiency can reach 82% and 87%, respectively. Plasma torches with tubular copper electrodes operating in reverse polarity make it possible to generate high-enthalpy plasma jets when using either argon as the plasma-forming gas, where the enthalpy can reach 6.5×10^6 J/kg, or nitrogen, where the enthalpy may reach 15.8×10^6 J/kg. This makes such plasma torches highly promising for spheroidization processes, enabling increased productivity and improved efficiency in treatment of the feedstock powder. From the standpoint of spheroidization efficiency, significant interest has been attracted by multi-electrode (three-cathode and six-cathode) plasma torch designs, where the degree of powder spheroidization can reach 96% or higher. However, despite the high plasma jet enthalpy of $36.7–46.1 \times 10^6$ J/kg, the reason for the low process throughput

in the spheroidization of both ceramic and metallic materials remains unclear. For zirconium oxide (ZrO_2), throughput does not exceed 0.75 kg/h, and for tungsten (W), it is around 1.2 kg/h. The analysis of plasma torch designs also showed that at present, the spheroidization of ceramic materials (primarily metal oxides) is most effectively achieved using cascade-type plasma torches operating with air or nitrogen as the plasma-forming gas. When combined with four-point radial powder injection, such systems may reach throughputs of up to 20 kg/h.

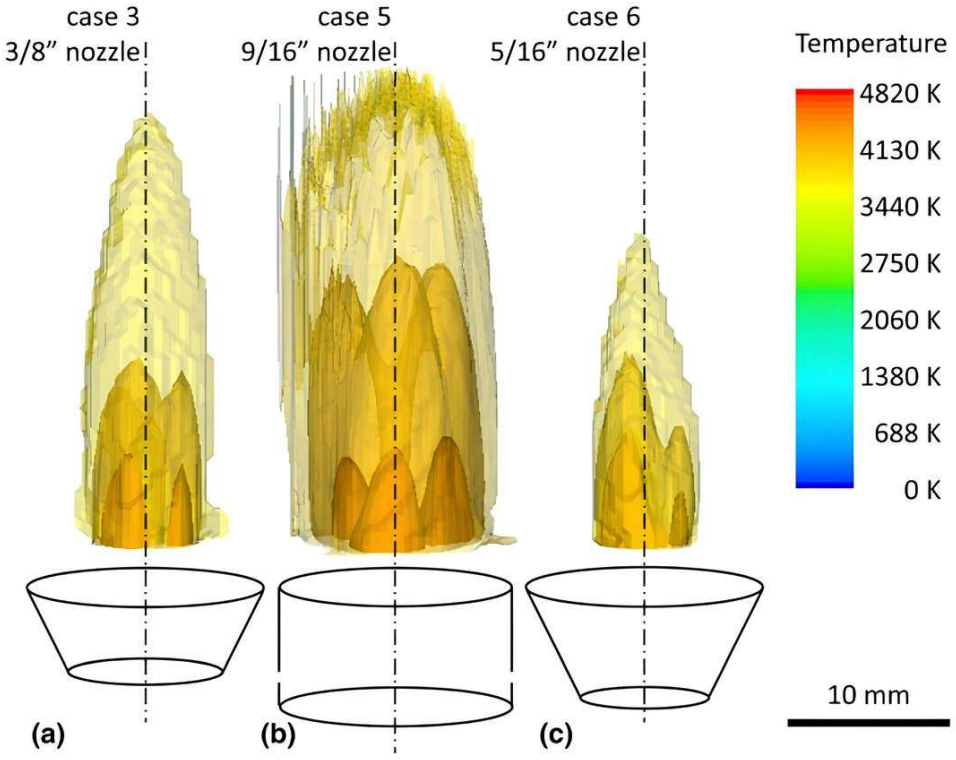

Figure 14. Tomographic 3D reconstruction of the temperature field in the plasma jet of the Axial III plasma torch using a new set of cathodes and anodes (operating time, $t < 5$ h). (a) Nozzle with a diameter of 3/8′′; (b) nozzle with a diameter of 9/16′′; (c) nozzle with a diameter of 5/16′′ (Reproduced from Ref. [43] with permission).

Table 2. Comparison of the thermal characteristics of direct current plasma torches.

Torch/scheme	Thermal efficiency, %	Arc voltage, V	Current, A	Plasma gas flow rate (slpm), *(g/s)	Plasma enthalpy, J/kg	Material	Spheroidization rate, %	Productivity, kg/h
Metco F4MB [86] (one cathode, one anode) Radial powder feeding into the plasma jet from a single point	-	*18 kW *28 kW	-	Ar (40)–He (15) Ar (40)–N_2 (3)	-	Al_2O_3 (–25 µm)	67 97	0.10 0.10

Continued on next page

Torch/scheme	Thermal efficiency, %	Arc voltage, V	Current, A	Plasma gas flow rate (slpm), *(g/s)	Plasma enthalpy, J/kg	Material	Spheroidization rate, %	Productivity, kg/h
Metco F4MB [87] (one cathode, one anode) Radial powder feeding into the plasma jet from a single point	-	30 30 30 *15 kW	400 545 655 -	Ar (40)–He (10) Ar (40)–He (10) Ar (40)–He (10) Ar (40)–He (15)	-	Stainless steel SS316L (+10, –150 μm) (+15, –45 μm)	80 77 86 80	0.30 0.30 0.30 2.8
Metco F4MB-XL [115] (one cathode, one anode)	49 60 60 54 58 61	32 38 42 32 37 41	600 600 600 800 800 800	Ar (40) Ar (60) Ar (80) Ar (40) Ar (60) Ar (80)	-	-	-	-
Metco SinplexPro [34] (cascade, one cathode, one anode)	51 73	89 81	500 500	Ar-H_2*(1.50) Ar–He *(1.44)	$15.1\cdot\times 10^6$ $20.1\cdot\times 10^6$	-	-	-
Khristianovich Institute of Theoretical and Applied Mechanics [88] (cascade, one cathode, one anode) Radial powder feeding into the plasma jet from four points	60–70	300	250	Air–CH_4 or N_2 (100)	-	Al_2O_3, ZrO_2–YSZ (+40, –120 μm)	-	20
Sichuan University [90] (three cathodes, one anode) Axial powder feeding into the plasma jet	40 41 44	129 138 170	3 × 120 3 × 120 3 × 120	N_2 (10) Nozzle: 12 mm N_2 (10) Nozzle: 17 mm N_2 (10) Nozzle: 22 mm	36.7 37.4 46.1	ZrO_2–YSZ (+10, –80 μm)	94.8 96.6 90.8	0.75
Hefei University [92] (six cathodes, one anode) Axial powder feeding into the plasma jet	-	20.5 25.8 30.7 34.2	6 × 450 6 × 390 6 × 390 6 × 390	Ar–He (20 Vol) Ar–He (20 Vol) Ar–He (40 Vol) Ar–He (60 Vol)	-	W (–45 μm)	62 59 73 96	1.2 1.2 1.2 1.2
WSP®H [93] (external copper anode), Radial feeding of powder into arc column	82	260	600	Ar (40)	-	-	-	-
MPN-04 [82] (external copper anode), Radial feeding of powder into arc column	73	40	45	Ar (3)	-	ZrO_2–7YSZ (–40 μm)	-	0.15

Continued on next page

Torch/scheme	Thermal efficiency, %	Arc voltage, V	Current, A	Plasma gas flow rate (slpm), *(g/s)	Plasma enthalpy, J/kg	Material	Spheroidization rate, %	Productivity, kg/h
RPT [61] (tubular copper cathode–anode)	74 70 87	202 137 193	140 120 80	Ar (120) Ar (60) Ar (150)	5.9×10^6 6.5×10^6 3.1×10^6	-	-	-
RPT [57,112] (tubular copper cathode–anode)	71 73 67	255 846 890	70 350 506	N_2 (50) N_2 (1050) N_2 (1050)	- 10.1×10^6 15.8×10^6	-	-	-

5. Conclusions

The present review highlights the following key findings:

1. As a result of the classification and analytical generalization of the current designs of DC plasma torches, it has been established that the use of plasma torches with "hot" tungsten electrodes has proven effective in industry when operating at high currents (up to 800 A) with gas mixtures based on argon with the addition of small amounts of helium, nitrogen, or hydrogen (mainly up to 5%–10%), where a high service life of the plasma torch is achieved and the electrode erosion rate does not exceed 1×10^{-12} kg/C. However, for modern tasks of spheroidizing powder material, it is necessary to use mixtures based not only on argon but also on nitrogen and helium, where the amount of the additive gas may exceed 20%. Under such conditions, the operation of tungsten electrodes becomes impossible, or, as in the case of using nitrogen as the plasma-forming gas, the erosion intensity increases fivefold.

Possible solutions to these challenges include the following:

(1) The use of local blowing of the tungsten cathode surface with a small amount of inert gas (argon), followed by passing the main gas flow (N_2, H_2, CH_4, CO_2, etc.) through the plasma to create a protective sheath around the tungsten cathode.

(2) The use of low-current (I = 70–300 A) and relatively high-voltage (U = 150–1000 V) plasma torch designs with "cold" autoemissive cathodes (tubular copper), where the cathode erosion intensity may decrease to $\sim 1 \times 10^{-14}$ kg/C.

2. Theoretical analysis of the physical processes occurring in a DC plasma arc during the interaction of the plasma with the dispersed material showed that the efficiency of spheroidization is determined by the set of plasma torch parameters (current, voltage, enthalpy of the plasma flow), gas velocity, and the particles' size and time of their stay in the plasma jet. Effective formation of a spherical morphology is ensured if the particles pass through the central high-temperature zone of the plasma jet, where they are uniformly heated and completely melted. A comparison of powder feeding schemes has shown that with radial feeding, the spheroidization efficiency is usually limited to 70%–82% at a plasma torch power of 15–18 kW and when using a plasma-forming mixture based on argon with nitrogen or helium. At the same time, when the plasma torch power is increased to 20–28 kW and, accordingly, the enthalpy of the plasma flow increases, the degree of spheroidization for radial feeding can rise to 86%–97%, which corresponds to certain high-power modes and experimental data on the treatment of oxide and metallic powder particles. In turn, axial feeding provides significantly better thermal conditions for particle heating, allowing more than 95% spherical particles to be achieved. In particular, in a three-cathode plasma torch with a power of 50 kW and axial feeding of ZrO_2–YSZ powder, a spheroidization degree of 96.6% was recorded when operating with

nitrogen plasma. When processing tungsten powder in an argon–helium plasma jet of a six-cathode plasma torch with a power of up to 80 kW, the degree of spheroidization reaches up to 96%.

3. Based on a review of current design and technological solutions, promising directions have been identified for improving the efficiency of plasma processing and the productivity of the spheroidization of ceramic and metallic materials. Plasma torches capable of generating a high-enthalpy plasma jet using nitrogen as the plasma-forming gas demonstrate the highest thermal efficiency for the spheroidization of ceramic materials, ensuring intensive and uniform particle melting. An additional way to enhance the degree of spheroidization and the overall process's productivity for both ceramic and metallic powders is to introduce the material directly into the arc column, where the energy density is significantly higher than in the peripheral regions of the plasma jet. Implementation of this approach requires the use of external electrodes, as in plasma torches of the MPN-04 and WSP® types, which opens up prospects for the substantial expansion of industrial applications of DC plasma torches in high-productivity powder spheroidization processes.

Another promising option for achieving a high degree of spheroidization of the feedstock powder is the use of plasma torch designs with axial powder injection, where this parameter can reach 96%–97%. However, existing laboratory-scale designs still require further optimization of gas-dynamic and thermal parameters to ensure stable and reliable operation, increase productivity, and improve the overall energy efficiency of the process.

Use of AI tools declaration

The authors declare they have not used artificial intelligence (AI) tools in the creation of this article.

Acknowledgments

The research was funded by: the Guangdong Academy of Sciences (GDAS, China)' Project of Science and Technology Development (2020GDASYL–20200301001) and the National Key Research and Development Program of China (2020YFE0205300).

Author contributions

Volodymyr Korzhyk: writing—original draft, conceptualization; Dmytro Strohonov: writing—original draft, conceptualization; Oleksii Tereshchenko: investigation, formal analysis, methodology; Peleshenko Sviatoslav: writing—review and editing, analysis; Oleg Ganushchak: writing—review and editing, investigation; Oleksii Demianov: writing—review and editing; Zhenlong Li: main supervision, project administration; Yu Chen: writing—review and editing, analysis.

Conflict of interest

The authors declare no conflict of interest.

References

1. Lanzutti A, Marin E (2024) The challenges and advances in recycling/re-using powder for metal 3D printing: A comprehensive review. *Metals* 14: 886. https://doi.org/10.3390/met14080886
2. Krishna R, Sreenivasan M, Lyutyk M, et al. (2025) Radio frequency plasma spheroidization of alumina as a feedstock material for ceramic 3D printing. *J Mater Eng Perform* 34: 2332–2343. https://doi.org/10.1007/s11665-024-09238-4
3. Kan W, Chiu L, Lim C, et al. (2022) A critical review on the effects of process-induced porosity on the mechanical properties of alloys fabricated by laser powder bed fusion. *J Mater Sci* 57: 9818–9865. https://doi.org/10.1007/s10853-022-06990-7
4. Bidare P, Jiménez A, Hassanin H, et al. (2022) Porosity, cracks, and mechanical properties of additively manufactured tooling alloys: A review. *Adv Manuf* 10: 175–204. https://doi.org/10.1007/s40436-021-00365-y
5. Boulos M (2011) Thermal plasma processing. *IEEE T Plasma Sci* 19: 1078–1089. https://doi.org/10.1109/27.125032
6. Fauchais P, Vardelle M, Goutier S (2019) Key challenges and opportunities in suspension and solution plasma spraying. *Plasma Chem Plasma Process* 35: 511–525. https://doi.org/10.1007/s11090-014-9594-5
7. Pawlowski L (2008) *The Science and Engineering of Thermal Spray Coatings*, Chichester: John Wiley & Sons. https://doi.org/10.1002/9780470754085
8. Trelles J, Chazelas C, Vardelle A (2009) Arc plasma torch modeling. *J Therm Spray Tech* 18: 728–752. https://doi.org/10.1007/s11666-009-9342-1
9. Wang L, Liu Y, Chang S (2016) Fabrication of spherical AlSi10Mg powders by radio frequency plasma spheroidization. *Metall Mater Trans A* 47: 2444–2453. https://doi.org/10.1007/s11661-016-3384-z
10. Samokhin A, Fadeev A, Alekseev N, et al. (2020) Spheroidization of Fe-based powders in plasma jet of DC arc plasma torch and application of these powders in selective laser melting. *Inorg Mater Appl Res* 11: 579–585. https://doi.org/10.1134/S2075113320030417
11. Getto E, Santucci R, Gibbs J, et al. (2023) Powder plasma spheroidization treatment and the characterization of microstructure and mechanical properties of SS 316L powder and L-PBF builds. *Heliyon* 9: e16583. https://doi.org/10.1016/j.heliyon.2023.e16583
12. Massard Q, Si-Mohand H, Cabrol E (2023) Study on the recycling of 100Cr6 powder by plasma spheroidization for laser powder bed fusion. *J Mater Res Technol* 27: 5889–5895. https://doi.org/10.1016/j.jmrt.2023.10.256
13. Kan W, Chiu L, Lim C, et al. (2022) A critical review on the effects of process-induced porosity on the mechanical properties of alloys fabricated by laser powder bed fusion. *J Mater Sci* 57: 9818–9865. https://doi.org/10.1007/s10853-022-06990-7
14. Brika S, Letenneur M, Dion C, et al. (2019) Influence of particle morphology and size distribution on the powder flowability and laser powder bed fusion manufacturability of Ti-6Al-4V alloy. *Addit Manuf* 31: 100929. https://doi.org/10.1016/j.addma.2019.100929
15. Bisset H, Van der Walt I, Havenga J, et al. (2015) Titanium and zirconium metal powder spheroidization by thermal plasma processes. *J S Afr Inst Min Metall* 115: 937–942. https://doi.org/10.17159/2411-9717/2015/v115n10a6

16. Eremin S, Anikin V, Kuznetsov D, et al. (2020) Spheroidization of iron powder in microwave and hybrid plasma torches. *J Non-ferr Met* 61: 199–206. https://doi.org/10.3103/S1067821220020042
17. Razumov N, Popovich A, Wang Q (2018) Thermal plasma spheroidization of high-nitrogen stainless steel powder alloys synthesized by mechanical alloying. *Met Mat Int* 24: 363–370. https://doi.org/10.1007/s12540-018-0040-8
18. Boulos M (1985) The inductively coupled R.F. (radio frequency) plasma. *Pure Appl Chem* 57: 1321–1352. https://doi.org/10.1351/pac198557091321
19. Boulos M (1992) RF induction plasma spraying: State-of-the-art review. *J Therm Spray Tech* 1: 33–40. https://doi.org/10.1007/BF02657015
20. Elaissi S, Trabelsi A, Alkallas F, et al. (2022) Energy efficiency enhancement of inductively coupled plasma torch: Computational study. *Materials* 15: 5213. https://doi.org/10.3390/ma15155213
21. Kameyama T, Sakanaka K, Motoe A, et al. (1990) Highly efficient and stable radio-frequency—Thermal plasma system for the production of ultrafine and ultrapure β-SiC powder. *J Mater Sci* 25: 1058–1065. https://doi.org/10.1007/BF03372203
22. Boulos M, Fauchais P, Pfender E (2023) *Handbook of Thermal Plasmas*, Switzerland: Springer Nature. https://doi.org/10.1007/978-3-319-12183-3
23. Safronov A, Vasileva O, Dudnik Y, et al. (2018) Use of alternating-current plasma torch for processing potentially hazardous substances. *High Energy Chem* 52: 319–323. https://doi.org/10.1134/S0018143918040136
24. Surov A, Popov S, Popov E et al. (2017) Multi-gas AC plasma torches for gasification of organic substances. *Fuel* 203: 1007–1014. https://doi.org/10.1016/j.fuel.2017.02.104
25. Wei X, Xu F, Bennett A, et al. (2023) Numerical analysis of direct-current (DC) plasma processing for high-efficient steel surface modification. *Int J Adv Manuf Technol* 124: 2215–2228. https://doi.org/10.1007/s00170-022-10548-x
26. Qiu J, Yu D, Li Y, et al. (2020) Design and characteristics of a triple-cathode cascade plasma torch for spheroidization of metallic powders. *Plasma Sci Technol* 22: 115503. https://doi.org/10.1088/2058-6272/aba8ed
27. Samokhin A, Alekseev N, Astashov A, et al. (2019) Synthesis and processing of powder materials in DC arc thermal plasma. *J Phys Conf Ser* 1393: 012126. https://doi.org/10.1088/1742-6596/1393/1/012126
28. Zaini I, Svanberg R, Sundberd D, et al. (2023) A pilot-scale test of plasma torch application for decarbonising the steel reheating furnaces. *TSEB* 40: 101766. https://doi.org/10.1016/j.tsep.2023.101766
29. Seo J, Hong B, Choi S, et al. (2013) Numerical design study on a high-powered segmented-type arc plasma torch for a high-enthalpy supersonic plasma wind tunnel. *J Korean Phys Soc* 62: 250–257. https://doi.org/10.3938/jkps.62.250
30. Chaturvedi V, Ananthapadmanabhann P, Chakravarthy Y, et al. (2014) Thermal plasma spheroidization of aluminum oxide and characterization of the spheroidized alumina powder. *Ceram Int* 40: 8273–8279. https://doi.org/10.1016/j.ceramint.2014.01.026
31. Fauchais P, Heberlein J, Boulos M (2013) *Thermal Spray Fundamentals: From Powder to Part*, New York: Springer. https://doi.org/10.1007/978-0-387-68991-3

32. Peng H, Shikai Y, Fangl Y, et al. (2007) Effect of plasma spheroidization process on the microstructure and crystallographic phases of silica, alumina and nickel particles. *Plasma Sci Tech* 9: 611–615. https://doi.org/10.1088/1009-0630/9/5/20
33. Liu S, Trelles J, Li C, et al. (2022) A review and progress of multiphase flows in atmospheric and low pressure plasma spray advanced coating. *Mater Today Phys* 27: 100832. https://doi.org/10.1016/j.mtphys.2022.100832
34. Mauer G (2022) Development of plasma parameters for the manufacture of MCrAlY bond coats by low-pressure plasma spraying using a cascaded torch. *Adv Eng Mater* 24: 2200856. https://doi.org/10.1002/adem.202200856
35. Szente R, Munz J, Drouet M (1992) Electrode erosion in plasma torches. *Plasma Chem Plasma Process* 12: 327–343. https://doi.org/10.1007/BF01447029
36. Mauer G (2024) Multiple electrodes and cascaded nozzles: A review of the evolution of modern plasma spray torches. *J Therm Spray Tech* 34: 484–494. https://doi.org/10.1007/s11666-024-01909-x
37. Sadek A, Ushio M, Matsuda F (1990) Effect of rare earth metal oxide additions to tungsten electrodes. *Metall Trans A* 21: 3221–3236. https://doi.org/10.1007/BF02647317
38. Coudert J, Planche M, Fauchais P (1995) Characterization of DC plasma torch voltage fluctuations. *Plasma Chem Plasma Process* 16: 211–227. https://doi.org/10.1007/BF01512636
39. Duan Z, Heberlein J (2002) Arc instabilities in a plasma spray torch. *J Therm Spray Tech* 11: 44–51. https://doi.org/10.1361/105996302770348961
40. Schein J, Zierhut J, Dzulko M, et al. (2007) Improved plasma spray torch stability through multi-electrode design. *Contrib Plasma Phys* 47: 498–504. https://doi.org/10.1002/ctpp.200710064
41. Vardelle A, Moreau C, Themelis N, et al. (2015) A perspective on plasma spray technology. *Plasma Chem Plasma Process* 35: 491–509. https://doi.org/10.1007/s11090-014-9600-y
42. Bagathi M, Vaßen R, Guillon O, et al. (2025) Coating characteristics of plasma-sprayed ceramic thermal barrier coatings on internal diameter (ID) surfaces. *J Therm Spray Tech* 34: 2918–2938. https://doi.org/10.1007/s11666-025-02042-z
43. Zimmermann S, Mauer G, Rauwald K, et al. (2021) Characterization of an axial-injection plasma spray torch. *J Therm Spray Tech* 30: 1724–1736. https://doi.org/10.1007/s11666-021-01235-6
44. Marqués J, Forster G, Schein J (2009) Multi-electrode plasma torches: Motivation for development and current state-of-the-art. *Open Plasma Phys J* 2: 89–98. https://doi.org/10.2174/1876534300902010089
45. Perambadur J, Rat V, Niane T, et al. (2024) Simulation of the Axial III Plus plasma torch and its arc fluctuations. *J Therm Spray Tech* 33: 2526–2547. https://doi.org/10.1007/s11666-024-01827-y
46. Ruelle C, Goutier S, Rat V, et al. (2024) Influence of nozzle diameter on electric arc dynamics and coating properties in a cascaded-anode plasma torch. *J Therm Spray Tech* 33: 756–770. https://doi.org/10.1007/s11666-023-01706-y
47. Dombrovskii L, Isakaev E, Senchenko V, et al. (2012) Efficiency of particle acceleration, heating, and melting in high-enthalpy plasma jets. *High Temp* 50: 145–153. https://doi.org/10.1134/S0018151X12020046
48. Zhang J, Shao P, Wang X, et al. (2023) Improving weld penetration by two-TIG arc activated via mixing oxygen into shielding gas. *Int J Adv Manuf Technol* 125: 169–181. https://doi.org/10.1007/s00170-022-10703-4

49. Belevtsev A, Goryachev S, Isakaev E, et al. (2016) Lifetime of the thermoemission cathodes of nitrogen plasma generators. *High Temp* 54: 789–795. https://doi.org/10.1134/S0018151X16040052
50. Belevtsev A, Goryachev S, Isakaev E, et al. (2013) Experimental study of the near-electrode plasma–tungsten cathode system in high-current atmospheric-pressure nitrogen arcs. *High Temp* 51: 583–593. https://doi.org/10.1134/S0018151X13050027
51. Baeva M, Benilov M, Zhu T, et al. (2022) Modelling and experimental evidence of the cathode erosion in a plasma spray torch. *J Phys D Appl Phys* 55: 365202. https://doi.org/10.1088/1361-6463/ac791c
52. Nemchinsky V (2012) Cathode erosion in a high-pressure high-current arc: calculations for tungsten cathode in a free-burning argon arc. *J Phys D Appl Phys* 45: 135201. https://doi.org/10.1088/0022-3727/45/13/135201
53. Pershin L, Mitrasinovic A, Mostaghimi J (2013) Treatment of refractory powders by a novel, high enthalpy DC plasma. *J Phys D Appl Phys* 46: 224019. https://doi.org/10.1088/0022-3727/46/22/224019
54. Solonenko O, Gulyaev I, Smirnov A (2011) Thermal plasma processes for production of hollow spherical powders: Theory and experiment. *J Therm Spray Tech* 6: 219–234. https://doi.org/10.1299/jtst.6.219
55. Park S, Kim D, Kim M, et al. (2013) Numerical analysis of a hollow electrode plasma torch with a reversed polarity discharge for radioactive waste treatment. *J Korean Phys Soc* 63: 1746–1754. https://doi.org/10.3938/jkps.63.1746
56. Zhukov M, Zasypkin I (2007). *Thermal Plasma Torches*, Cambridge: Cambridge International Science Publishing Ltd.
57. Yang I, Choi M, Nam J, et al. (2019) Experimental and numerical analyses of a hollow electrode plasma torch with inter-electrodes and reversed polarity *J Korean Phys Soc* 74: 465–472. https://doi.org/10.3938/jkps.74.465
58. Camacho S (1988) Industrial-worthy plasma torches: State-of-the-art. *Pure Appl Chem* 60: 619–632. https://doi.org/10.1351/pac198860050619
59. Yin Z, Yu D, Wen Y, et al. (2021) Numerical investigation on the flow characteristics of a reverse-polarity plasma torch by two-temperature thermal non-equilibrium modelling. *Plasma Sci Technol* 23: 095402. https://doi.org/10.1088/2058-6272/ac0770
60. Rao L, Rivard F, Carabin P (2013) Thermal plasma torches for metallurgical applications. 4th International Symposium on High-Temperature Metallurgical Processing, 57–65. https://doi.org/10.1002/9781118663448.ch8
61. Yin Z, Yu D, Zhang Q, et al. (2021) Experimental and numerical analysis of a reverse-polarity plasma torch for plasma atomization. *Plasma Chem Plasma Process* 41: 1471–1495. https://doi.org/10.1007/s11090-021-10181-8
62. Zhang X, Hou X, Hao Z, et al. (2022) Research on spheroidization of tungsten powder from three different raw materials. *Materials* 15: 8449. https://doi.org/10.3390/ma15238449
63. Soucy G, Jurewicz J, Boulos M (1994) Mixing study of the induction plasma reactor: Part II. Radial injection mode. *Plasma Chem Plasma Process* 14: 59–71. https://doi.org/10.1007/BF01448737
64. Soucy G, Jurewicz J, Boulos M (1994) Mixing study of the induction plasma reactor: Part I. Axial injection mode. *Plasma Chem Plasma Process* 14: 43–58. https://doi.org/10.1007/BF01448736

65. Goel S, Björklund S, Curry N, et al. (2020) Axial plasma spraying of mixed suspensions: A case study on processing, characteristics, and tribological behavior of Al_2O_3–YSZ coatings. *Appl Sci* 10: 5140. https://doi.org/10.3390/app10155140
66. Sharivker S, Krasnov A (1966) Possibility of obtaining spherical particles by radial feeding of fine powder into a plasma jet. *Powder Metall Met Ceram* 5: 173–177. https://doi.org/10.1007/BF00776219
67. Andreytsev A, Smyrnov I, Chornyi A, et al. (2021) Modeling the process of spheroidization powder particles by the plasma-arc method. *Appl Quest Math Modell* 4: 25–32. https://doi.org/10.32782/KNTU2618-0340/2021.4.2.2.2
68. Fialko N, Sherenkovskii J, Meranova N, et al. (2021) Establishing patterns in the effect of temperature regime when manufacturing nanocomposites on their heat-conducting properties. *East-Eur J Enterp Technol* 112: 21–26. https://doi.org/10.15587/1729-4061.2021.236915
69. Fialko N, Prokopov V, Meranova N, et al. (1994) Temperature conditions of particle–substrate systems in a gas-thermal deposition process. *Fiz Khim Obrab Mater* 2: 59–67. Available from: https://www.scopus.com/pages/publications/0028385421?origin=resultslist.
70. Andreytsev A, Smyrnov I, Chornyi A (2009) Analysis of the dynamics of fine particle motion during plasma spraying. *Zbirnyk Naukovykh Prats DETUT* 11: 100–103.
71. Kharlamov M, Krivtsun I, Korzhyk V (2014) Dynamic model of the wire dispersion process in plasma-arc spraying. *J Therm Spray Tech* 23: 420–430. https://doi.org/10.1007/s11666-013-0027-4
72. Zurabov V, Puzryakov A (1983) On the acceleration of powder particles during plasma spraying. *Phys Chem Materials Treat* 3: 52–55.
73. Haider A, Levenspiel O (1989) Drag coefficient and terminal velocity of spherical and nonspherical particles. *Powder Tech* 58: 63–70. https://doi.org/10.1016/0032-5910(89)80008-7
74. Boulos M (2016) The role of transport phenomena and modeling in the development of thermal plasma technology. *Plasma Chem Plasma Process* 36: 3–28. https://doi.org/10.1007/s11090-015-9660-7
75. Ozerskoi N, Silin A, Razumov N, et al. (2021) Optimization of EI961 steel spheroidization process for subsequent use in additive manufacturing: Effect of plasma treatment on the properties of EI961 powder. *Rev Adv Mater Sci* 60: 936–945. https://doi.org/10.1515/rams-2021-0078
76. Lokhov Y, Petrunichev V, Uglov A, et al. (1974) Heating and evaporation of particles in a low-temperature plasma jet. *Phys Chem Materials Treat* 6: 52–56.
77. Fialko N, Prokopov V, Sherenkovskij Y, et al. (1992) Mathematical simulation of 3D temperature fields in coatings during gas-thermal spraying of alloys prone to amorphous transformation. *Elektron Obrab Mater* 5: 20–23.
78. Ouyang H, Chen X, Huang B (2007) Influence of melt superheat on breakup process of close-coupled gas atomization. *Trans Nonferrous Metals Soc China* 17: 967–973. https://doi.org/10.1016/S1003-6326(07)60209-X
79. Matsumoto T, Fujii H, Ueda T, et al. (2005) Measurement of surface tension of molten copper using the free-fall oscillating drop method. *Meas Sci Technol* 16: 432–437. https://doi.org/10.1088/0957-0233/16/2/014
80. Mikhalev V, Petrunichev V (1968) Study of plasma jet velocities and the velocities of dispersed particles treated in it. *Phys Chem Materials Treat* 5: 22–27.
81. Lykov P, Baitimerov R, Safonov E, et al. (2013) Modeling of melt atomization process in a gas jet. *Bull South Ural Stat Univ* 2: 148–154.

82. Klinskaya-Rudenskaya N, Frishberg I, Tsymbalist M, et al. (1999) Investigation of the spheroidization of refractory powders with particle size 20–100 μm in a low-temperature plasma. *High Temp* 37: 26–30.
83. Prokopov V, Fialko N, Sherenkovskij Y, et al. (1992) Analysis of temperature conditions in the "coating–sublayer–substrate" system under gas-thermal spray coating of composite powders. *Elektron Obrab Mat* 2: 12–15.
84. Korzhik V (1992) Theoretical analysis of the conditions required for rendering metallic alloys amorphous during gas-thermal spraying. III. Transformations in the amorphous layer during the coating growth process. *Powder Metall Met Ceram* 31: 943–948. https://doi.org/10.1007/BF00797621
85. Fialko N, Prokopov V, Meranova N, et al. (1993) Thermal physics of gas-thermal coating formation processes: State of investigations. *Fiz Khim Obr Mater* 4: 83–93.
86. Iovane P, Borriello C, Pandolfi G, et al. (2025) Spheroidization of alumina powders for additive manufacturing applications by DC plasma technology. *Molecules* 30: 453. https://doi.org/10.3390/molecules30030453
87. Iovane P, Borriello C, Pandolfi G, et al. (2024) Thermal plasma spheroidization and characterization of stainless steel powders using direct current plasma technology. *Plasma* 7: 76–90. https://doi.org/10.3390/plasma7010006
88. Solonenko OP, Smirnov AV (2014) Advanced oxide powders processing based on cascade plasma. *J Phys Conf Ser* 550: 012017. https://doi.org/10.1088/1742-6596/550/1/012017
89. Goryachev S, Khromov M, Kavyrshin D, et al. (2021) Velocity and temperature of plasma jets and their change due to artificial optical inhomogeneities introduced into plasma. *High Temp* 59: 36–45. https://doi.org/10.1134/S0018151X2101003X
90. Qiu J, Yu D, Chen Y, et al. (2024) Controllable preparation of YSZ-STHS in arc plasma spheroidization: Exploring the plasma flow characteristics impact on powder quality. *Ceram Int* 50: 26569–26582. https://doi.org/10.1016/j.ceramint.2024.04.385
91. Wang C, Zhang Z, Xia W, et al. (2017) Direct observation of anode arc root behaviors in a non-transferred arc plasma device with multiple cathodes. *Plasma Chem Plasma Process* 37: 371–382. https://doi.org/10.1007/s11090-016-9782-6
92. Zhang Z, Wang C, Sun Q, et al. (2022) Spheroidization of tungsten powder by a DC arc plasma generator with multiple cathodes. *Plasma Chem Plasma Process* 42: 939–956. https://doi.org/10.1007/s11090-022-10250-6
93. Yushchenko K, Borisov Y, Pereverzev Y, et al. (1995) Microplasma spraying. *Proc Int Thermal Spray Conf* 14*:* 237–274.
94. Kombayev K, Khoshnaw F, Kozhakhmetov Y, et al. (2025) Microplasma sprayed tantalum coatings on Ti Grade 5 extra-low interstitials: Investigation of thickness and porosity control. *Coatings* 15: 464. https://doi.org/10.3390/coatings15040464
95. Borisov Y, Voynarovich S, Kislitsa A, et al. (2017) Development of microplasma spraying technology for restoring local damages of enamel coatings. *Paton Weld J* 7: 35–41. https://doi.org/10.15407/as2017.07.06
96. Borisov Y, Voynarovich S, Kislitsa A, et al. (2018) Application of the microplasma spraying method for manufacturing resistive heating elements. *Paton Weld J* 2: 42–47. https://doi.org/10.15407/as2018.02.07

97. Borisov Y, Korzhik V, Kunitskii Y, et al. (1986) Structural transformations in thermal spray coatings of Ni60Nb40 alloy during vacuum annealing. *Sov Powder Metall Metal Ceram* 25: 821–826.
98. Gu Y, Zhang W, Xu Y, et al. (2022) Stress-assisted corrosion behaviour of Hastelloy N in FLiNaK molten salt environment. *npj Mater Degrad* 6: 90. https://doi.org/10.1038/s41529-022-00300-x
99. Skorokhod A, Sviridova I, Korzhik V (1995) Effect of mechanical pretreatment of polyethylene terephthalate powder on the structural and mechanical properties of coatings made from it. *Mech Compos Mater* 30: 328–334. https://doi.org/10.1007/BF00634755
100. Han J, Shi Y, Guo J, et al. (2023) Porosity inhibition of aluminum alloy by power-modulated laser welding and mechanism analysis. *J Manuf Process* 102: 827–838. https://doi.org/10.1016/j.jmapro.2023.08.001
101. Fialko N, Dinzhos R, Sherenkovskii J, et al. (2021) Establishment of regularities of influence on the specific heat capacity and thermal diffusivity of polymer nanocomposites of a complex of defining parameters. *Eastern-European J Enterp Technol* 114: 34–39. https://doi.org/10.15587/1729-4061.2021.245274
102. Borisov Y, Korzhyk V (1998) Internal stresses in plasma coatings with an amorphous structure. *Proc Int Thermal Spray Conf* 1: 693–697.
103. Skorokhod A, Sviridova I, Korzhik V (1994) Structural and mechanical properties of polyethylene terephthalate coatings as affected by mechanical pretreatment of powder during preparation. *Mech Compos Mater* 30: 455–463.
104. Fialko N, Dinzhos R, Sherenkovskaya G, et al. (2022) Influence on the thermophysical properties of nanocomposites of the duration of mixing of components in the polymer melt. *Eastern-European J Enterp Technol* 116: 25–30. https://doi.org/10.15587/1729-4061.2022.255830
105. Borisov Y, Kislitsa A, Voynarovich S, et al. (2018) Investigation of electric and energy characteristics of the plasmatron in microplasma spraying with wire materials. *Paton Weld J* 9: 23–28. https://doi.org/10.15407/as2018.09.04
106. Jenista J, Takana H, Nishiyama H, et al. (2011) Integrated parametric study of a hybrid-stabilized argon–water arc under subsonic, transonic and supersonic plasma flow regimes. *J Phys D Appl Phys* 44: 435204. https://doi.org/10.1088/0022-3727/44/43/435204
107. Ondac P, Maslani A, Hrabovsky M (2016) Investigation of the arc–anode attachment area by utilizing a high-speed camera. *Plasma Phys Technol* 3: 1–4. https://doi.org/10.14311/ppt.2016.1.1
108. Dudik J (2022) Morphological and structural changes of ceramic powders during plasma spraying. Available from: https://dspace.cvut.cz/handle/10467/105396.
109. Project Soft (2025) Plasma torch for thermal spraying. Available from: http://www.projectsoft.sk/en/plazma-systems.php.
110. Ross D, Burgess A (1996) Plasma Jet Converging System. United States Patent 5,556,558.
111. Mettech (2025) Axial III Plasma Spray System. Available from: https://www.mettech.com/coating-equipment/axial-III-plasma-spray-system.php.
112. Lee N, Lee D, Kim S, et al. (2025) Experimental and numerical investigations on the operational characteristics of a hollow electrode plasma torch with an exit nozzle and reverse polarity discharge structure. *J Korean Phys Soc* 86: 1135–1147. https://doi.org/10.1007/s40042-025-01386-7

113. Korzhyk V, Strohonov D, Gao S, et al. (2025) Production of spherical Inconel 625 powder for additive manufacturing by plasma-arc wire atomization: Influence of non-transferred and transferred arc modes on fine powder yield. *Adv Sci Technol Res J* 19: 109–123. https://doi.org/10.12913/22998624/209176
114. Gao S, Korzhyk V, Strohonov D, et al. (2025) Evaluation of the possibility of obtaining spherical powders of titanium alloy Ti-6Al-4V by supersonic reverse polarity plasma torch for use in additive manufacturing. *Adv Sci Technol Res J* 19: 434–448. https://doi.org/10.12913/22998624/205855
115. Baeva M, Zhu T, Kewitz T, et al. (2021) Self-consistent cathode–plasma coupling and role of the fluid flow approach in torch modeling. *J Therm Spray Tech* 30: 1737–1750. https://doi.org/10.1007/s11666-021-01261-4

AIMS Press